Technische Universität München
TUM School of Life Sciences

Microscale properties of iron minerals in redoximorphic soils

Lydia Emily Pohl

Vollständiger Abdruck der von der TUM School of Life Sciences der Technischen Universität München zur Erlangung einer

Doktorin der Naturwissenschaften (Dr. rer. nat.)

genehmigten Dissertation.

Vorsitz: Prof. Dr. Jörg Völkel

Prüfer*innen der Dissertation:

1. Prof. Dr. Dr. h.c. Ingrid Kögel-Knabner
2. Prof. Dr. Thilo Rennert

Die Dissertation wurde am 27.09.2023 bei der Technischen Universität München eingereicht und durch die TUM School of Life Sciences am 20.12.2023 angenommen.

Zusammenfassung

Unter dem allgemeinen Begriff “redoximorphe Böden“ lassen sich verschiedene Bodentypen zusammenfassen, die durch redoximorphe Eigenschaften gekennzeichnet sind. Diese Böden entstehen vor allem durch den wiederholten Wechsel zwischen reduzierenden und oxidierenden Bedingungen in der Bodenmatrix. Länger andauernde Phasen der Wassersättigung führen zur mikrobiellen Reduktion von dreiwertigem Eisen (Fe^{III}) zu zweiwertigen Eisen (Fe^{II}) und der damit einhergehenden Auflösung von Fe-Oxiden und (Oxy-)Hydroxiden (vereinfacht als Fe-Oxide bezeichnet). Die freigesetzten Fe^{2+}-Ionen können mit der Bodenlösung verlagert und unter oxischen Bedingungen (z.B. in Poren oder Wurzelkanälen) wieder als Fe^{III}-Oxide ausgefällt werden. Infolgedessen bilden sich die charakteristischen redoximorphen Merkmale, wie z.B. Rostflecken, Konkretionen, oder, unter sauerstoffarmen Bedingungen, Bleichung.

Fe-Oxide haben einen entscheidenden Einfluss auf die Nährstoffverteilung in Böden und gehören zu den wichtigsten Sorbenten von organischer Bodensubstanz (*engl. soil organic matter, SOM*), Nährstoffen (z. B. Phosphor) und Schadstoffen. Die Adsorptionskapazität hängt hierbei hauptsächlich von der Kristallinität der Fe-Oxide ab, die jedoch durch den Einbau von Kationen beeinflusst werden kann. Der ständige Wechsel in den Redoxbedingungen führt jedoch zu einer wiederholten Auflösung und Neubildung der Fe-Oxide und damit zu einer ständigen Veränderung der Oxid-Verteilung und der entsprechenden Adsorbate. In Folge dessen ist die räumliche Verteilung von Fe-Oxiden in redoximorphen Böden, sowie die mikroskalige Verteilung der Adsorbate sehr dynamisch. Die zugrundeliegenden Prozesse werden häufig anhand makroskopischer Parameter charakterisiert, die nur begrenzt zur Beschreibung der mikroskaligen Heterogenität geeignet sind. So sind Rückschlüsse auf die räumliche Verteilung auf den Probenahmebereich der untersuchten Bodenprobe beschränkt, der von einigen Zentimetern bis zu Dezimetern reichen kann. Im Gegensatz dazu bieten bildgebende Verfahren wie die nanoskalige Sekundärionen-Massenspektrometrie (NanoSIMS) Einblicke in die räumliche Verteilung der Elementhäufigkeiten mit einer Auflösung von bis zu ~ 100 nm.

In der vorliegenden Dissertation wurde ein Bildanalyseprotokoll entwickelt, das es ermöglicht, räumliche Unterschiede in der Elementverteilung mit NanoSIMS zu visualisieren und zu quantifizieren. Hierbei wurden verschieden Fe-Minerale untersucht, die charakteristisch für redoximorphe Böden sind. Die Analysen wurden an synthetischen Proben unter Laborbedingungen (Studie I), synthetischen Proben unter natürlichen Bedingungen (Studie II) und an natürlichen, ungestörten Proben (Studie III) durchgeführt.

In Studie I wurde untersucht, ob die Konzentration von Aluminium (Al), in Al-substituierten Goethiten durch NanoSIMS quantifiziert werden kann. Bei Goethit handelt es sich um eines der am häufigsten auftreten Fe-Oxide in redoximorphen Böden, wobei das Fe^{III} häufig durch Al substituiert ist. Für die Analysen wurden Al-substituierte Goethite mit Al-Konzentrationen von 0.1, 3 und 7 % synthetisiert. Die Ergebnisse zeigen deutlich, dass die ansteigende Al-Konzentration durch die NanoSIMS Messungen widergespiegelt wird. Durch eine statistische Bildauswertung konnten zudem in der Probe mit der höchsten Al-Substitution (7 %) räumliche Muster identifiziert werden, die eine statistisch signifikant niedrigere Al-Konzentration aufweisen. Durch XRD und Mößbauer-Spektroskopie wurde in dieser Probe Hämatit als zweite Fe-Oxide nachgewiesen. Hämatit baut bekanntermaßen weniger Al im Vergleich zu Goethit in die Mineralstruktur ein, so dass folglich die räumlichen Muster in den NanoSIMS-Bildern auf verschiedene Fe-Oxide zurückgeführt werden konnten.

Der Schwerpunkt von Studie II und III lag vor allem auf der Quantifizierung der räumlichen Verteilung von SOM in Abhängigkeit der darunter liegenden Mineralphase. Hierfür wurden in Studie II Kunststoffstäbe, die mit synthetischen, gut kristallinem Fe-Oxiden und Mangan(Mn)-Oxiden beschichten waren, für 30 Tage in einem redoximorphen Boden installiert. Unter reduzierenden Bedingungen reagiert das Mn-Oxid mit Fe^{2+}-Ionen aus der Bodenlösung und es kommt zur Bildung von natürlichen Fe-Oxiden auf der Oberfläche des Kunststoffstabes. Durch die entwickelte Bildanalyse konnte gezeigt werden, dass die schlecht kristallinen, natürlich gebildeten Fe-Oxide einen fast doppelt so hohen Bedeckungsgrad mit SOM aufwiesen, im Vergleich zu den gut kristallinen, synthetischen Fe-Oxiden.

In Studie III wurde zusätzlich gezeigt, dass die SOM-Verteilung in Fe-Konkretionen nicht nur von der Mineralphase abhängt, sondern auch von der Mikroporosität beeinflusst wird. Hierfür wurden in Studie III Konkretionen untersucht, die sich in einem ehemaligen Mangrovengebiet nach der Trockenlegung des Bodens entlang von reliktischen Wurzelkanäle gebildet haben. Die Ergebnisse zeigen, dass die mineralische Phase in unmittelbarer Nähe des Wurzelkanals fast vollständig mit SOM assoziiert ist. Darüber hinaus war die organische Substanz in isolierten Poren nachweisbar, deren Durchmesser unterhalb der Größe der meisten Mikroorganismen liegt und deren mikrobielle Zugänglichkeit somit erschwert wird. Der so eingeschlossene Kohlenstoff kann daher als räumlich stabilisiert angesehen werden kann und zur langfristigen Stabilisierung von Kohlenstoff in Fe-Konkretionen beitragen.

Die Ergebnisse der Dissertation konnten somit zeigen, dass NanoSIMS durch eine entsprechende Bildanalyse zum Prozessverständnis in redoximorphen Böden beitragen kann. Das entwickelte Bildanalyseprotokoll ermöglicht die Identifizierung und Quantifizierung von räumlichen Mustern, die Bewertung von Zusammenhängen zwischen verschiedenen Elementen und die Untersuchung des Einflusses von mineralogischen Eigenschaften auf die Verteilung von z. B. SOM. Diese Ergebnisse tragen dazu bei, unser Wissen über die komplexen, mikroskaligen Prozesse in redoximorphen Böden zu erweitern, und können somit Einblicke in die Stabilität und Dynamik der Fe-Mineralien in diesen Böden geben.

Summary

The generic term “redoximorphic soils” refers to various soil types characterized by their redoximorphic features. The formation and development of these soils are caused by the repeated transition between reducing and oxidizing conditions. Prolonged periods of water saturation lead to the microbial reduction of ferric (Fe^{III}) to ferrous (Fe^{II}) iron and the accompanied dissolution of iron (Fe) oxides and (oxy-) hydroxides (collectively referred to as Fe oxides). The released Fe^{2+} ions can be translocated with the soil water and immobilized again as Fe^{III} oxide under oxic conditions. As a result, characteristic morphological soil patterns are formed, like redox depletions (i.e., localized zones of “decreased” pigmentation) in anaerobic horizons and redox concentrations (i.e., localized zones of enhanced pigmentation due to an accumulation of Fe minerals) in oxic horizons.

Fe oxides have a decisive impact on the nutrient distribution in soils. They are among the most important minerals for the sorption of soil organic matter (SOM), nutrients (e.g., phosphorus), and pollutants. The adsorption capacity is mainly a function of their crystallinity, which can be influenced by the incorporation of a wide range of cations. However, the continuous change in redox conditions leads to a repeated dissolution and neoformation of Fe oxides in redoximorphic soils and thus alters the Fe oxide distribution and the associated adsorbates. Consequently, it is still challenging to determine the spatial distribution of Fe oxides in redoximorphic soils, as well as the microscale distribution of the adsorbates. The underlying processes are often characterized by macroscopic parameters, which provide only limited information to describe the heterogeneity at the microscale. Conclusions regarding the spatial distribution are consequently limited to the sampling area of the analyzed bulk soil sample, which can range from a few centimeters to decimeters. In contrast, imaging techniques like nanoscale secondary ion mass spectrometry (NanoSIMS) offer insights into the spatial distributions of elemental abundances on single mineral particles or in undisturbed soil samples with a high lateral resolution (~100 nm).

In this dissertation, an image analysis protocol was developed that allows us to visualize and quantify spatial differences of elemental distribution with NanoSIMS on Fe minerals, which are characteristic of redoximorphic soils. The analyses were performed on synthetic samples under lab conditions (Study I), synthetic samples under natural conditions (Study II), and on natural, undisturbed samples (Study III).

Study I focused on the analysis of aluminum (Al) as the most commonly observed substituent of Fe^{III} and investigated if the concentration of Al with increasing Al substitution in Fe oxides can be obtained by NanoSIMS. Therefore, goethite, as one of the most common Fe oxides in redoximorphic soils, was synthesized with Al concentrations of 0.1,

3, and 7%. The results demonstrated that NanoSIMS could accurately estimate the concentration of incorporated Al. The statistical analysis of the images and reassignment of single pixels characterized as ‘outliers’ allowed us to additionally identify distinct spots with a lower Al concentration. These spots were found only in the sample with the highest Al-substitution (7%), which simultaneously exhibited shares of hematite detected by XRD and Mössbauer spectroscopy. Goethite always exceeds the concentration of Al in contrast to hematite. Consequently, the spatial patterns in the NanoSIMS images can be ascribed to different Fe oxides.

Due to the high lateral resolution of NanoSIMS, particularly for light elements, such as carbon, the focus of Study II and III was primarily on quantifying the spatial distribution of SOM as a function of the underlying mineral phase. For this purpose, in Study II, plastic bars, which were coated with synthetic, well-crystalline Fe oxide and manganese (Mn) oxide, were installed for 30 days in redoximorphic soil. The Mn oxide coating was supposed to react under reducing conditions with Fe^{2+} from the soil solution and lead to the formation of new, naturally formed Fe oxides on the surface of the bar. Due to the investigated image analysis, it could be shown that the poorly crystalline, naturally formed Fe oxides exhibited nearly twice the SOM coverage than the well-crystalline, synthetic Fe oxides introduced into the soil.

In Study III, it was additionally shown that in redox concentrations, the SOM distribution is not only dependent on the mineral phase but also influenced by the microporosity. In Study III, relict redox concentrations, which have formed in a former tidal wetland along relict root channels, were embedded in resin to maintain the undisturbed soil structure and investigated by NanoSIMS. The image analysis revealed that the mineral phase in close vicinity to the relict root channel was almost completely associated with SOM. In addition, the SOM was detectable in single, isolated pores with a diameter below the size of most microorganisms. As a result, the microbial accessibility might be hampered, and the entrapped carbon can thus be considered as spatially stabilized. This demonstrated that NanoSIMS can contribute to understand the processes which lead to the known long-term carbon stabilization within redox concentrations.

The presented dissertation demonstrated that NanoSIMS, in combination with the appropriate image analysis, is a valuable adjunct to conventional methods to understand the functioning of Fe minerals in redoximorphic soils. The developed image analysis protocol enables the identification and quantification of spatial patterns, the assessment of associations between various elements, and the investigation of the influence of mineralogical properties on the distribution of, for example, SOM. These findings contribute to advancing our knowledge of the complex processes occurring at the

microscale in soil systems and can thus provide insights into the Fe mineral stability and dynamic in redoximorphic soils.

Content

Abbreviations

µCT	X-ray computed microtomography
AsB	Angle-selective Backscatter
EDX	energy dispersive X-ray spectroscopy
FTIR	Fourier-transform infrared spectroscopy
HySpex	hyperspectral imaging
IRIS	Indicator of Reduction in Soils
NanoSIMS	nanoscale secondary ion mass spectrometry
OC	organic carbon
ROI	region of interest
SEM	scanning electron microscope
SOM	soil organic matter
VNIR	visible near-infrared
XRD	X-ray diffraction

List of publications and contributions

The presented doctoral dissertation is based on the following three first-authored research articles. All studies are attached in the appendix.

Study I	**Lydia Pohl, Angelika Kölbl, Florian Werner, Carsten W. Mueller, Carmen Höschen, Werner Häusler, Ingrid Kögel-Knabner (2018): Imaging of Al/Fe ratios in synthetic Al-goethite revealed by nanoscale secondary ion mass spectrometry. Rapid Communications in Mass Spectrometry 32, 619-628.**
Contribution:	I conducted the data evaluation and wrote the manuscript.
Objectives:	To reveal the concentration of aluminum (Al) with increasing Al substitution in synthetic goethite by NanoSIMS.
Methods:	We synthesized Al-substituted goethite samples with increasing Al concentrations of 0.1, 3, and 7%. The samples were analyzed by NanoSIMS and the bulk spectroscopic methods XRD, FTIR, and Mössbauer spectroscopy.
Results:	XRD and FTIR confirmed the increasing substitution of Al for iron (Fe) within the goethite structure. A linear correlation between the molar Al/Fe ratio derived by total digestion and the corresponding $^{27}Al^{16}O^{-}$ /$^{56}Fe^{16}O^{-}$ ratio derived from NanoSIMS was verified. In addition, shares of hematite were revealed with Mössbauer spectroscopy in the sample with the highest Al-substitution (7%). Statistical analysis of the NanoSIMS data and reassignment of single pixels characterized as 'outliers' allowed us to identify distinct spots with a lower $^{27}Al^{16}O^{-}$ /$^{56}Fe^{16}O^{-}$ ratio within the corresponding NanoSIMS images. In combination with the results from XRD and Mössbauer spectroscopy, these spots were characterized as hematite.
Conclusions:	The study confirmed that absolute element contents can be obtained by NanoSIMS if calibration standards with appropriate matrix composition are used. Combining statistical image analysis and bulk spectroscopic techniques allowed us to visualize the distribution of different Fe oxides at the nanoscale, i.e., to determine the size and distribution of hematite within a goethite-dominated sample.

Study II **Kristof Dorau*, Lydia Pohl*, Christopher Just, Carmen Höschen, Kristian Ufer, Tim Mansfeldt, Carsten W. Mueller (2019): Soil Organic Matter and Phosphate Sorption on Natural and Synthetic Fe Oxides under in Situ Conditions. Environmental Science and Technology 53, 13081-13087.**

Contribution: I conducted the NanoSIMS data analysis and interpretation and co-wrote the manuscript.

Objectives: Assessment of soil organic matter (SOM) and phosphorus (P) sorption on natural and synthetic Fe oxides at the microscale under in situ conditions in redoximorphic soil.

Methods: We installed plastic bars that have been coated with synthetic Fe or manganese (Mn) oxides for 30 days in redoximorphic soil. The Mn oxide coating was supposed to react under reducing conditions with Fe^{2+} from the soil solution and lead to the precipitation of new, naturally formed Fe oxides on the surface of the bar. These 'natural' Fe oxides and the remaining 'synthetic' Fe oxides were investigated by NanoSIMS to study the distribution of Fe ($^{56}Fe^{16}O^-$), SOM ($^{12}C^{14}N^-$), and phosphorus ($^{31}P^{16}O_2^-$).

Results: NanoSIMS image analysis revealed a close association of Fe, SOM, and P, resulting in a mean coverage of 71 ± 25 for $^{12}C^{14}N^-$ and 68 ± 33 for $^{31}P^{16}O_2^-$ for the natural Fe oxides, while the mean coverage of the synthetic Fe oxides is lower with 43 ± 28 for $^{12}C^{14}N^-$ and 47 ± 35 for $^{31}P^{16}O_2^-$. Ion ratios of sorbent ($^{56}Fe^{16}O^-$) and sorbate ($^{12}C^{14}N^-$ and $^{31}P^{16}O_2^-$) were smaller along natural compared with synthetic Fe oxides.

Conclusions: Natural and synthetic Fe oxides rapidly sequestered SOM and P (i.e., within 30 days), but newly naturally formed Fe oxides sorbed more SOM and P than synthetic Fe oxides.

---

* equal contribution

Study III **Lydia Pohl, Angelika Kölbl, Daniel Uteau, Stephan Peth, Werner Häusler, Luke Mosley, Petra Marschner, Rob Fitzpatrick, Ingrid Kögel-Knabner (2021): Porosity and organic matter distribution in jarositic phyto tubules of sulfuric soils assessed by combined µCT and NanoSIMS analysis. Geoderma 399, 115124**

Contribution: I contributed to the study design, conducted the fieldwork and laboratory analysis, carried out the data evaluation, and wrote the manuscript.

Objectives: To elucidate the porosity, spatial extension, and organic matter distribution of jarositic phyto tubules (i.e., preserved root fragments enclosed by tubular accumulations of jarosite), which have formed along relict mangrove root channels in sulfuric soil.

Methods: Soil cores containing jarositic phyto tubules were taken from a former tidal wetland. The soil cores were embedded in resin and analyzed by µCT, EDX-SEM, and NanoSIMS.

Results: Jarositic phyto tubules could be differentiated into zones with either high or low concentrations of jarosite at distances of < 0.5 mm and 0.5–1.9 mm from the relict root channel, respectively. NanoSIMS analyses revealed a closer association between jarosite and organic matter in the zone with high jarosite concentration. The pore space in the immediate vicinity of the relict root channel was almost completely filled by jarosite, which led to a mean pore diameter of 525 nm ± 496 nm. Consequently, the root-derived organic matter was completely encapsulated and therefore disconnected from the bulk soil matrix.

Conclusions: After re-submergence of the acidic soil material, the encapsulation of root-derived organic matter with jarosite may strongly reduce its availability as substrate for microbial reduction processes and therefore retard remediation processes.

1. Introduction

The generic term “redoximorphic soils” describes different soil types characterized by their redoximorphic features (Dorau et al., 2020; Gasparatos et al., 2019). The formation and development of these soils are caused by the repeated transition between reducing and oxidizing conditions (Reddy and DeLaune, 2008). During prolonged periods of water saturation (e.g., due to ascending ground water or flooding), the oxygen (O_2) content in the soil decreases, and microorganisms utilize terminal electron acceptors other than O_2, including nitrate, manganese, ferric iron, and sulfate (Dorau et al., 2020; Hansel et al., 2015). The reduction from ferric (Fe^{III}) to ferrous (Fe^{II}) iron is accompanied by the dissolution of iron (Fe) oxides and (oxy-) hydroxides (collectively referred to as Fe oxides) and the release of Fe^{2+} ions into the soil solution (Weber et al., 2006). Depending on the soil pH, Fe^{II} is more soluble than the oxidized species and can be translocated with the soil water (Winkler et al., 2018). In the presence of O_2 (e.g., in larger pores, root channels, or after drainage), the Fe^{II} is immobilized again by oxidation as Fe^{III} oxides.

The described processes occur in a number of soils in the landscape, e.g., in wetland soils, such as tidal marshes or mangrove wetlands, seasonally or temporarily flooded soils due to rising groundwater levels or heavy rainfall events and managed wetlands, such as paddy soil (Inglett et al., 2005; Reddy and DeLaune, 2008). Since Fe oxides have a significant effect on soil color, the influence of the periodic or permanent saturation with water leads to characteristic color patterns, which are readily recognizable in the field. Permanently water-saturated and anaerobic soil horizons exhibit redox depletions (i.e., localized zones of “decreased” pigmentation), while the oxic horizon is characterized by redox concentrations (i.e., localized zones of enhanced pigmentation due to an accumulation of Fe oxides) (Schoeneberger et al., 2012). As a result, unique morphological soil patterns are formed, which are used as diagnostic indicators in many soil classification systems (AG Boden, 2005; IUSS Working Group WRB, 2015). For example, reducing conditions caused by prolonged periods of groundwater saturation result in the formation of gleyic properties (in Gleysols), while periods of temporary saturation with surface water favor stagnic properties (in Planosols, Plinthosols, and Stagnosols) (IUSS Working Group WRB, 2015). Even though water is essential for the formation of redoximorphic features, they were even described in soils that are no longer temporarily or permanently saturated with water (Greenberg and Wilding, 1998; Lindbo et al., 2010; Vepraskas, 2001). For example, if a site has been artificially drained, the observed features may persist and remain as relict redoximorphic features in the soil (Vepraskas and Lindbo, 2012). Thus, soils can exhibit redoximorphic features, even if they are no longer redox active.

1.1. Redox dynamics and mineralogical (trans)formation of Fe oxides in redoximorphic soils

The most common Fe oxides in redoximorphic soils of temperate climates are goethite and ferrihydrite (Bigham et al., 2002). Ferrihydrite is formed by rapid oxidation of Fe^{II}, e.g., in soil horizons with seasonal groundwater fluctuation, and is therefore often assumed to be the first formed Fe phase in soils (Bigham et al., 2002). Goethite (α-FeOOH) is generally formed by (i) weathering of Fe-containing primary minerals, (ii) abiotic and microbial oxidation of dissolved Fe^{II} ions in reduced/anaerobic soils, which results in the precipitation of Fe^{III}-oxide minerals, and (iii) aging processes of less crystalline Fe oxides (Bigham et al., 2002; Cornell and Schwertmann, 2003; Weber et al., 2006).

Fe oxides are among the most important minerals for the sorption of soil organic matter (SOM), nutrients (e.g., phosphorus), and pollutants in soils (e.g., Borch and Fendorf, 2007; Eusterhues et al., 2003; Kaiser and Guggenberger, 2000; Mansfeldt and Overesch, 2013). Besides environmental factors like pH, the adsorption capacity of Fe oxides is mainly a function of their crystallinity and the corresponding surface area. Less crystalline Fe oxides like ferrihydrite are known to have a higher specific surface area and thus a higher adsorption capacity towards, e.g., phosphate (Parfitt, 1989) or SOM (Eusterhues et al., 2005) in comparison to more crystalline oxides like goethite. However, the crystallinity can be influenced by the incorporation of a wide range of cations (e.g., Alvarez et al., 2015; Trolard et al., 1995), which are present in the soil solution. Due to its ubiquitous distribution in soils and its high relative abundance, aluminum (Al) is the most commonly observed substituent of Fe^{III} in Fe oxides (Bigham et al., 2002). The extent of substitution directly influences the mineralogical properties because Al has a smaller ionic radius than Fe. For goethite, the incorporation of Al, e.g., causes a decrease in the unit-cell dimension (Schulze, 1984). This results in a change of the morphology, a decrease of the particle size, an increase of the specific surface area (Schulze and Schwertmann, 1984; Schwertmann, 1984) and was, e.g., observed to directly influence the adsorption capacity regarding phosphorus (Ainsworth and Sumner, 1985; Hsu et al., 2020).

However, the continuous change in redox conditions leads to a repeated dissolution and neoformation of Fe oxides in redoximorphic soils and thus the mineralogical properties. Under reducing conditions, less crystalline Fe oxides are preferential microbially reduced relative to more crystalline forms (Postma, 1993; Roden, 2003), which leads to the release of dissolved Fe^{2+} into the soil solution. The Fe^{2+} is either removed from the soil, re-oxidized, and subsequently re-precipitated as Fe oxides of low crystallinity or incorporated

into ferrous-bearing minerals (Thompson et al., 2011; Winkler et al., 2018). Depending on the specific soil hydrology, this results in either a relative increase (Thompson et al., 2006) or a decrease (Coby et al., 2011; Vogelsang et al., 2016b) of the overall Fe mineral crystallinity over time. For example, under prolonged and repetitive anaerobic conditions, the sorption of Fe^{2+} onto Fe solid phases has been shown to accelerate the transformation of less crystalline Fe oxides to more crystalline Fe oxides, such as goethite (Kukkadapu et al., 2003; Vogelsang et al., 2016a; Williams and Scherer, 2004). As a result, changing redox conditions also alter the distribution of adsorbates associated with Fe oxides. Nutrients or pollutants may be mobilized (Chen et al., 2020; Mansfeldt and Overesch, 2013; Peretyazhko and Sposito, 2005) and translocated with the soil solution.

1.2 Investigation of the microscale distribution of Fe oxide associated elements in redoximorphic soils

Due to the temporal and spatial variability in redox conditions of redoximorphic soils, it is still challenging to provide reliable information on the alteration of the Fe mineral phase, as well as the microscale distribution of adsorbates. In the past, a large number of studies has been carried out to investigate the fate of Fe oxides under changing redox conditions in redoximorphic soils (e.g., Mansfeldt et al., 2012; Thompson et al., 2006; Vogelsang et al., 2016a; Winkler et al., 2018). The conclusions regarding the underlying processes are often based on macroscopic parameters, which provide only insufficient information to describe the heterogeneity at the microscale (Baveye et al., 2018). For example, the correlation between Fe oxides and carbon (Anthony and Silver, 2020) or heavy metals (Thomas and Strobel, 2022) is still often only characterized by statistical relationships between the elemental and the Fe oxide content of the sample. Conclusions regarding the spatial distribution are therefore limited to the sampling area of the analyzed bulk soil sample, which can range from a few centimeters to decimeters. In addition, the Fe oxide content is often determined by selective chemical extractions, which have restricted precision (Mansfeldt et al., 2012; Schwertmann, 1964), especially if the Fe oxides are associated with organic carbon (Fisher et al., 2021).

In particular, for redoximorphic soils, in which the spatiotemporal dynamic leads to an incessant change of the micro-scale mineral properties and the spatial distribution of the adsorbates, the classical bulk methods are therefore only suitable to reflect these dynamics to a limited extent. In contrast, imaging techniques like nanoscale secondary ion mass spectrometry (NanoSIMS) allow the measurement of elemental abundances on single mineral particles or in undisturbed soil samples while offering a high lateral resolution at the microscale of about 100 nm in particular for light elements like, e.g.,

carbon (Mueller et al., 2013). This enables, e.g., the spatial distribution of SOM to be studied as a function of the spatial distribution of the underlying mineral. Even though NanoSIMS became a widely used methodology for the investigation of soil samples (Mueller et al., 2012; Mueller et al., 2013; Mueller et al., 2017b), only a few studies were carried out, which investigated Fe oxides in redoximorphic soils by NanoSIMS (e.g., Schlüter et al., 2022). Even fewer studies deal with the spatial distribution of adsorbates (Possinger et al., 2020; Rennert et al., 2014). Rennert et al. (2014) investigated the distribution of SOM in Fe and manganese (Mn) oxide accumulations from a Stagnosol. They demonstrated that the Mn oxides and the transitional zones between Fe and Mn oxides were enriched in SOM, while SOM was absent within the pure Fe-accumulation zones (Rennert et al., 2014). Possinger et al. (2020) additionally demonstrated that the spatial correlation between Fe oxides and SOM is related to the water saturation cycle frequency (i.e., frequency of water table presence and recession cycles). In soils with a lower water saturation frequency, the Fe is spatially more correlated to SOM, while in soils with a higher water saturation cycle frequency, the SOM was more correlated to Al oxides (Possinger et al., 2020). These two studies already suggest that classical bulk methods might imply a preferential association of Fe oxides with SOM, whereas imaging techniques showed that the spatial distribution of SOM can vary considerably at the microscale in redoximorphic soils. As demonstrated in the mentioned studies, it is possible to directly visualize these spatial relationships in the range of a few micrometers by using NanoSIMS.

2. Objectives and approaches

Each NanoSIMS image consists of a large number of single pixels, which can be considered as spatially resolved point measurements on a regular spatial grid and can be statistically evaluated accordingly. In this dissertation, an image analysis protocol was developed that allows not only to visualize spatial differences of elemental distribution with NanoSIMS but also to evaluate them statistically and quantitatively. It will be demonstrated that the developed image analysis protocol enabled qualitative and quantitative conclusions about spatial patterns of elemental distributions on Fe minerals, which are characteristic of redoximorphic soils. To illustrate the variability of possible applications, analyses were performed on synthetic samples under lab conditions (Study I), synthetic samples under natural conditions (Study II), and natural, undisturbed samples (Study III).

Study I

In redoximorphic soils, the Al substitution in goethite is mainly restricted to 0 – 15%, while goethite formed in acidic, highly weathered, and non-redoximorphic soils may have higher Al concentrations up to 32% (Fitzpatrick and Schwertmann, 1982). The degree of Al substitution can vary spatially within the soil profile depending on the respective formation conditions. If the Fe oxides form, e.g., in the vicinity of Al-bearing clay minerals, the degree of substitution can be increased due to released Al ions (Schwertmann et al., 2000b). In contrast, if the goethite is spatially accumulated within the redoximorphic soil profile (e.g., in redox concentrations), the degree of Al substitution is lower and only amounts up to 10% (Fitzpatrick and Schwertmann, 1982) were observed. The content of incorporated Al has a determining influence on the mineralogical properties and thus also affects the adsorption capacity of Fe oxides. For example, an Al content of 10% is sufficient to increase the adsorption capacity of goethite towards phosphate by 2.1 times in comparison to non-substituted goethite (Hsu et al., 2020). Consequently, the concentration of nutrients can vary spatially and may be lower in presumed accumulation areas with high goethite content like redox concentrations but a low degree of Al substitution, in comparison to areas in the surrounding soil, where less goethite with a higher substitution grade might be found.

So far, the quantification of the Al substitution is mainly derived from X-ray diffraction (XRD) analysis and based on the detectable change in crystallinity (i.e., the unit-cell parameters) as a result of the Al incorporation (Kukkadapu et al., 2001; Neumann et al., 2014; Schulze, 1984). A spatial analysis of the potentially formed gradients within the

intact soil matrix is therefore not possible. In contrast, NanoSIMS would be suitable to study these gradients in undisturbed soil samples and, even more advantageous, to potentially interpret them quantitively. So far, only a few studies exist that deal with a quantitative interpretation of NanoSIMS results (e.g., Gabitov et al., 2013; Thomen et al., 2020). Several aspects must be taken into account for a quantitative evaluation of the ion count ratios derived from NanoSIMS (Hatton et al., 2012; Herrmann et al., 2007; McMahon et al., 2006). For example, ion count ratios can be biased by differences in the ionization efficiency due to the variable crystallinity of the sample matrix (Gabitov et al., 2013). The incorporation of Al and the associated changes in the mineralogical properties of goethite could therefore lead to a misleading change in the detectable ion count ratios with an increasing concentration of Al. Therefore, the reliability of the detected ion count ratios and whether they reflect the concentration of incorporated Al has to be verified. Consequently, the aim of Study I was to investigate if the concentration of incorporated Al in goethite can be obtained by using NanoSIMS. As such, the approach included:

Study I: Imaging of Al/Fe ratios in synthetic Al-goethite revealed by nanoscale secondary ion mass spectrometry

i) The synthesis of Al-substituted goethite with an Al concentration up to 7% to reflect the typical low substitution grade in redoximorphic soils.
ii) The analyses of the goethite samples with standard bulk spectroscopic methods (e.g., XRD and Mössbauer spectroscopy) and NanoSIMS.
iii) The correlation of the $^{27}Al^{16}O^-/^{56}Fe^{16}O^-$ ratio obtained from NanoSIMS with the molar ratio derived from total digestion to verify NanoSIMS as a possible tool to determine the Al substitution in goethite at the microscale.

Study II

One method to investigate the fate of Fe oxides in redoximorphic soils under in situ conditions is the “Indicator of Reduction in Soils” (IRIS) Method (Jenkinson and Franzmeier, 2006). This method employs white PVC bars coated with synthetic Fe oxides that remain in the soil for a previously defined time. Upon removal, it is possible (I) to quantify the loss of Fe oxides from the bar surface to compare the reductive conditions during the time of installation (Dorau et al., 2016) or (II) to analyze the remaining Fe oxides regarding the adsorption of trace metals or nutrients (Dorau and Mansfeldt, 2016).

Due to a bar length of approx. 60 cm, the capillary fringe can be examined separately from soil horizons above and below the groundwater table. More interestingly, even the

formation of natural Fe oxides can be investigated by using bars that are coated with Mn oxides. Under reducing conditions, the Mn (acting as oxidants) reacts with the dissolved Fe^{II} (acting as reductant) of the soil solution. The Mn^{2+} is removed from the PVC surface, and new Fe^{III} oxides are precipitated (Dorau et al., 2016; Dorau and Mansfeldt, 2016). The newly formed Fe oxides along the Mn bar can be referred to as “natural” Fe oxides because they have formed under field conditions. So far, the IRIS method has been used to investigate the adsorption behavior of Fe oxides towards trace metals and phosphorus (Dorau and Mansfeldt, 2016). This was achieved by chemical extraction of the oxide coatings from the entire bar length (Dorau and Mansfeldt, 2016) and, thus, eliminates the possibility of any spatial analyses at the microscale.

By combining the IRIS method with NanoSIMS, it should be possible to keep the spatial information and to differentiate the distribution and spatial extent of the adsorbed SOM or phosphorus derived from natural soil solution on natural and synthetic Fe oxides by simultaneously defining the timescale needed to form the investigated organo-mineral associations. To test this approach, in Study II, redox bars were placed in redoximorphic soil and analyzed afterwards using NanoSIMS. As such, the approach included:

Study II: Soil organic matter and phosphate sorption on natural and synthetic Fe oxides under in situ conditions

i.) The installation of Fe and Mn redox bars in a Gleysol for 30 days.
ii.) Analyses of the ‘naturally’ formed Fe oxides and the remaining ‘synthetic’ Fe oxides by using NanoSIMS to study the distribution of phosphorus and SOM at the microscale.
iii.) Comparison between the ‘natural’ and ‘synthetic’ Fe oxides regarding the coverage with phosphorus and SOM.

Study III

Under anoxic conditions, like in the permanently saturated subsoil of redoximorphic soils, the stability of Fe oxides is primarily controlled by the activity of Fe^{III}-reducing bacteria (Weber et al., 2006). A special exception are sulfidogenic environments, where the reduction of Fe oxides is additionally controlled by the reaction with biogenic formed hydrogen sulfide (Hansel et al., 2015; Weber et al., 2006). In the presence of sulfate, as likely in seawater-influenced environments (e.g., estuarian or mangroves), and available organic carbon (OC), the activity of sulfate-reducing bacteria leads to the formation of hydrogen sulfides (Alongi et al., 2001; Holmer et al., 1994). The hydrogen sulfide reacts

with the Fe oxides, which leads to the abiotic reduction of Fe^{III} and the formation of Fe sulfides (Hansel et al., 2015). Consequently, pyrite (FeS_2) is the most common Fe mineral in the subsoil of redoximorphic, sulfidogenic environments like mangrove sediments (Johnston et al., 2009; Moeslundi et al., 1994; Noël et al., 2014; Otero et al., 2009). Its spatial distribution in the subsoil is mainly dependent on the availability of OC and is therefore increased by a high root density (Ferreira et al., 2007). The release of root exudates or the decay of dead root material leads to the stimulation of sulfate-reducing bacteria in the sediments and can lead to the enhanced formation of pyrite on the root surface (Roychoudhury et al., 2003) or along root channels (Rabenhorst and Haering, 1989). If the subsoil is aerated (e.g., via natural or artificial drainage), the pyrite is oxidized and causes sulfuric acid to be produced and the formation of sulfuric material ($pH < 4$) (Fitzpatrick et al., 2012; Michael et al., 2015; Poch et al., 2009). Concomitantly, this leads to the formation of Fe sulfates, in particular jarosite [$KFe_3(SO_4)_2(OH)_6$)].

Once acidified, the soils constitute a significant environmental risk due to their low pH value and the associated mobilization of heavy metals (Fältmarsch et al., 2008). To increase the pH value of the soils and to re-establish anaerobic conditions mandatory for pyrite formation, re-saturation has been considered as a possible remediation strategy (Creeper et al., 2015a; Johnston et al., 2014; Kölbl et al., 2019; Wong et al., 2016). Comparable to the prior natural formation conditions of pyrite, the remediation success depends on the availability of OC to increase the activity of sulfate-reducing bacteria. The microbial accessibility of potential OC sources in the soil is influenced by the pore size, the soil structure (Baldock and Skjemstad, 2000; Kravchenko and Guber, 2017), and the pore connectivity (Young et al., 2008). Due to the prior spatial association of pyrite with the root surface, jarosite is often described in the field as a pale-yellow accumulation along root channels (Creeper et al., 2015b; Kölbl et al., 2019) and can be designated as jarositic phyto tubules (Brewer and Sleeman, 1988). Consequently, the physical and chemical properties of the surrounding soil matrix were modified due to the precipitation of jarosite in the pore space, and the encapsulated root residues may have become unavailable for microbial access. The effect of the jarosite formation on the pore space and the accessibility of the OC is unexplored at present, and its importance under natural conditions is unknown.

Therefore, the focus of Study III was to evaluate the porosity, spatial extension, and organic matter distribution of jarositic phyto tubules, which have formed along relict mangrove root channels in sulfuric soil. As such, the approach of Study III included:

Study III: Porosity and organic matter distribution in jarositic phyto tubules of sulfuric soils assessed by combined µCT and NanoSIMS analysis

i.) The analysis of undisturbed soil cores with a jarositic phyto tubule in its center by using a combination of X-ray computed microtomography (µCT) and NanoSIMS.

ii.) The characterization of the jarositic phyto tubules in two distinct zones with either high or low concentration of jarosite based on the porosity information derived by µCT.

iii.) The analysis of the spatial association of jarosite with SOM depending on the porosity of the jarosite and distance from the relict root channel.

3. Material and Methods

Chapter 3 summarizes the main material and methods for all studies. A more detailed presentation is available in the respective publication in the appendices.

3.1. Sample material

The results of the present thesis are based on a combination of natural and synthetic samples. In the following paragraphs, the mineral synthesis or sampling is described for each study separately.

For Study I, three goethite samples with increasing Al substitution (0.1, 3, and 7%) were synthesized according to Schwertmann and Cornell (2000). Briefly, 0, 50, and 120 mL of an aluminate solution (0.3125 M) were mixed with 180, 174, and 165 mL, respectively, of 5 M KOH solution. Immediately afterwards, 100 mL of 1 M $Fe(NO_3)_3$ solution was added and filled up to 2 L with distilled water. The solutions were placed in an oven at 70°C and shaken once per day. After 14 days, the mineral phase was separated by centrifugation, washed twice with 400 mL 1 M KOH to remove extra Al, adjusted to pH 7.5 with 1 M HCl, washed with distilled water, and then freeze-dried.

For Study II, Mn and Fe redox bars were manufactured by applying a synthetic mineral suspension on the roughened PVC bar surface following the procedure by Dorau and Mansfeldt (2015) for the Mn redox bars and by Jenkinson and Franzmeier (2006) and Rabenhorst and Burch (2006) for the Fe redox bars. For the Mn redox bar, the birnessite suspension was synthesized according to Händel et al. (2013). For the Fe redox bars, the ferrihydrite suspension was synthesized by precipitation from a ferric chloride solution by adding KOH and stored for 7d to cause the formation of goethite via mineralogical alteration (Rabenhorst and Burch, 2006). The redox bars were 60 cm in length (Ø 21 mm) with the lower 50 cm coated and were installed for 30 days in a Mollic Gleysol (Dorau et al., 2016) located in the district of Recklinghausen (Germany) (Figure 1). A push probe with a soil auger having the same length and width was predrilled into the soil. In addition, a metal protection sheath was simultaneously pushed with the PVC bar into the soil to ensure that the oxide-coated surface was not in contact with any other part of the soil profile. The sheath was removed after installation. After the installation period, the bars were carefully removed by digging a soil pit. Adhering soil material from the bar's surface was removed with deionized water, and the bars were stored dry afterward for the subsequent analyses. The production of the redox bars and the installation in the field was performed by Kristof Dorau (University of Cologne).

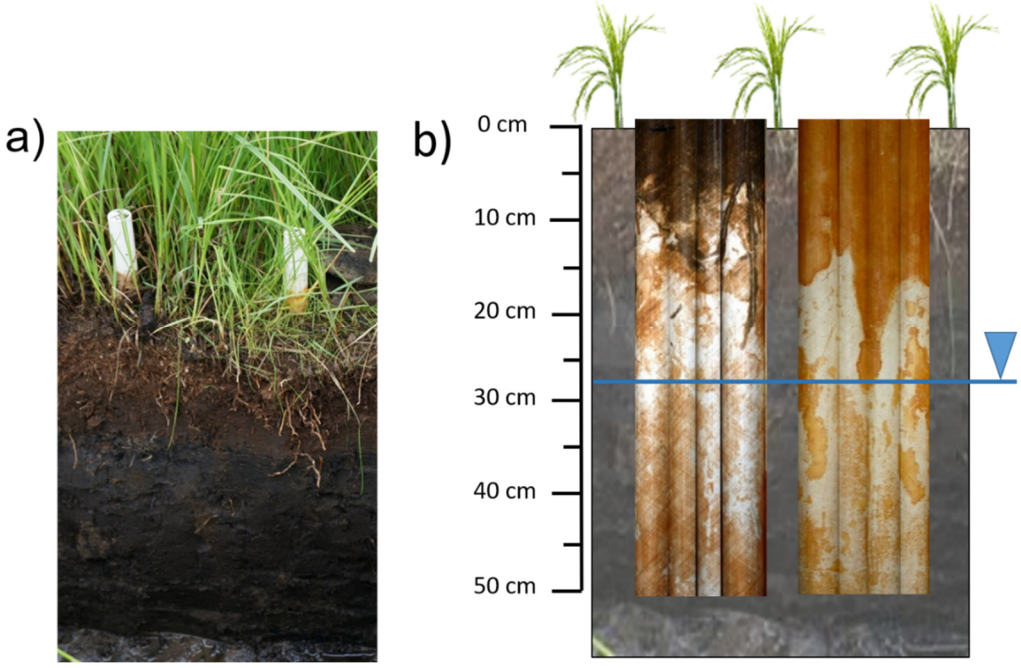

Figure 1: (a) Profile of the Mollic Gleysol with the installed Mn and Fe redox bars. (b) An image of the Mn (left) and Fe (right) redox bar after the installation time of 30 days. For the image, a picture was taken of each 90° section, and the distorted images were cropped together. The blue line indicates the mean water table depth (adapted from Dorau et al., 2019; Study II).

For Study III, samples were taken from a former tidal wetland in the Barker Inlet estuary close to Adelaide (Australia). Based on the Australian Soil Classification (Isbell and National Committee on Soil and Terrain, 2016) and WRB identification keys (IUSS Working Group WRB, 2015), the soil profile is classified as a Peaty, Sulfuric, Hypersalic Hydrosol and Salic Fluvisol (Hyperthionic, Drainic), respectively. The main characteristic of the subsoil are pale yellow coatings and infillings of jarosite, which have formed around relict mangrove roots and the root channels and are designated as jarositic phyto tubules (Brewer and Sleeman, 1988) (Figure 2). Bulk sandy sulfuric material was taken from a strongly acidic soil horizon (pH_{H2O} = 2.5) at a soil depth of 80-145 cm. In addition, soil cores (1.5 cm diameter, 1.5 cm height), each with a jarositic encapsulated relict mangrove root in its center, were taken and embedded in resin to maintain the undisturbed, natural soil structure (see Chapter 3.3.1).

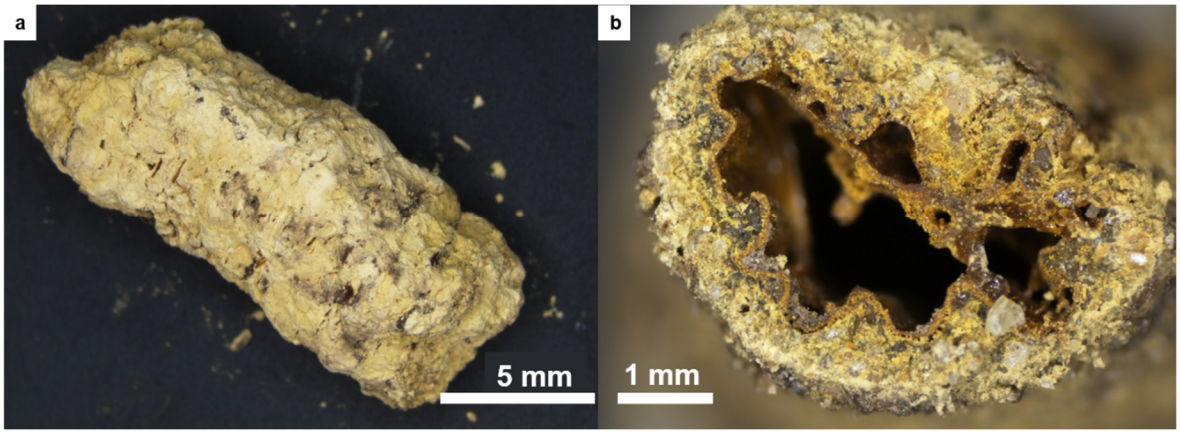

Figure 2: (a) Top view and (b) cross-section of a handpicked phyto tubule. The preserved mangrove root structures in the middle are still clearly visible (Pohl et al., 2021; Study III).

3.2. Mineralogical and elemental composition

Table 1 gives an overview of the applied methods regarding the mineralogical and elemental characterization of the sample material of the three presented studies:

Table 1: Overview of the applied methods for Study I, II, and III.

Parameter	**Method**	**Study**
C and N content	Dry combustion at 1000 °C, Elemental Analyzer (EuroEA Elemental Analyzer 3000, Wegberg, Germany)	III
Total elemental composition	Total digestion with HF/$HClO_4$ followed by ICP-OES (Vista Pro CCD Simultaneous, Varian, Palo Alto, USA)	I, III
Mineralogical characterization	X-ray diffraction (PW1070 diffractometer, Philips, Eindhoven, The Netherlands)	I, III
	X-ray diffraction (D8 Advance, Bruker, Karlsruhe, Germany)	II
	Fourier-transform infrared spectroscopy (Nicolet iS10, Thermo Fisher Scientific, Dreieich, Germany)	I
Identification of Fe oxides	Mössbauer spectroscopy	I, III

3.3. Microscale analyses

3.3.1 Sample preparation for NanoSIMS analysis

For Study I, a 0.1 mg subsample of each synthesized goethite sample and an additional hematite sample (Fe_2O_3, pro analysi; Merck, Darmstadt, Germany) was dispersed in 10 mL of deionized water. Then, 100 µL of the dispersion was placed on a carbon wafer and dried overnight.

For Study II, a square from the surface (3 x 3 mm, at 20 cm soil depth) was cut out of the Mn and Fe redox bar by a hand saw to analyze the in situ formed organo-mineral associations. Additional material was cut out from two redox bars, which were not installed in the soil profile, and used as reference material to ensure a distinction between soil organic matter and the PVC material.

For Study III, the intact soil cores were initially dehydrated using a stepwise increasing concentration of acetone (from 30% to 100% (v/v)), following the impregnation with a mixture of Procure-Araldite:acetone (1:3, to 1:1 (vl:vl)) and finally with pure Procure-Araldite (Procure-Araldite Embedding Kit, ProSciTech, Kirwan, Australia). The cores were cured at 60 °C for at least 48 h (Mueller et al., 2017a). One core was cut horizontally into thin slices (thickness: ~1 mm) using a diamond saw (Struers Dicsplan TS). Two slices were glued onto a glass disc of 25.4 mm diameter and polished carefully (Figure 3).

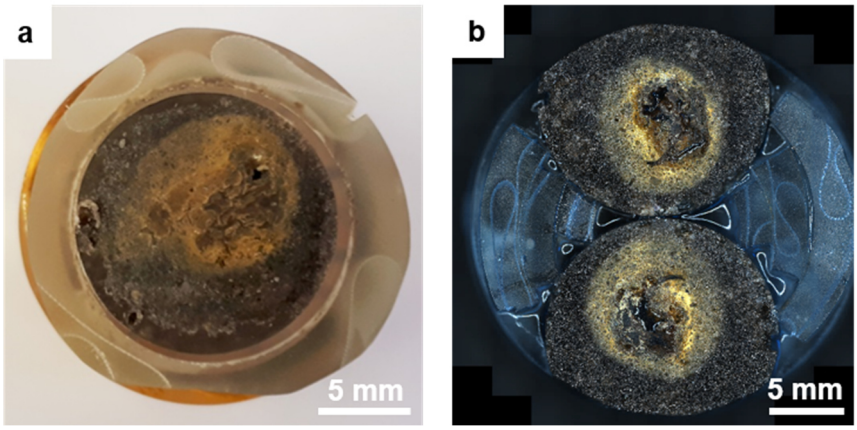

Figure 3: (a) Top view of an embedded soil core with relict root cannel in the centre and (b) 2 core slices on a glass disc prepared for EDX-SEM and NanoSIMS analysis (dark-field image) (adapted from Pohl et al., 2021; Study III).

Prior to the NanoSIMS analysis, all samples were examined with reflected-light-microscopy (ZeissAxio Imager Z2m microscope (Zeiss, Jena, Germany)) to create an overview image and determine regions of interest. The selected regions were scanned with a higher magnification (up to 50x) to map the sample surface for the location of appropriate spots for NanoSIMS measurement. In Study III, additional Angle-selective

Backscatter (AsB) images and energy dispersive X-ray spectroscopy (EDX) maps were taken with an ULTRA plus field emission scanning electron microscope (Zeiss, Jena, Germany).

The NanoSIMS measurements were recorded with a Cameca NanoSIMS 50L (Gennevilliers, France) using a high-energy cesium (Cs^+) ion beam (~1.2 pA). Prior to the measurements, the samples were coated with Au/Pd (~ 30 nm, SCD 005 sputter coater; Baltec GmbH, Germany). In Study II, the additional use of the electron flood gun was necessary to compensate for charging effects due to the nonconductive, subjacent bar material. Charging describes the deposit of Cs^+ ions on the sample surface due to the non-conductive sample material, resulting in low counts of detectable negative secondary ions (Pett-Ridge and Weber, 2012).

In all studies, the primary ion beam was used with a primary ion impact energy of 16 keV and focused onto the sample surface with a lateral resolution of ~100 nm. The emitted secondary ions were distinguished by their mass-to-charge ratio in a double-focusing magnetic sector mass spectrometer and detected using electron multipliers. Up to 7 masses can be detected simultaneously. Depending on the respective research question of the study, the following secondary ions were recorded: $^{16}O^-$, $^{12}C^-$, $^{12}C_2^-$, $^{12}C^{14}N^-$, $^{28}Si^-$, $^{32}S^-$, $^{27}Al^{16}O^-$, $^{31}P^{16}O_2^-$, $^{56}Fe^{16}O^-$ and $^{56}Fe^{16}O_2^-$. Fe and Al do not form single negatively charged secondary ions due to their low electron affinity and were measured consequently as oxygen-containing cluster ions (Kilburn and Wacey, 2015). The detailed measurement conditions regarding the field of view, pixel dimension, number of planes, and applied dwell time for all three studies are summarized in Table 2.

Table 2: Overview of the NanoSIMS measurement conditions for Study I, II, and III

Field of view	Pixel dimension	Number of planes	Dwell time	Study
20 µm x 20 µm	256 x 256 pixels	1 plane	30 ms/pixel	I
40 µm x 40 µm	512 x 512 pixels	10 planes	1 ms/pixel	II
30 µm x 30 µm	400 x 400 pixels	10 planes	1 ms/pixel	III

3.3.2 Image analysis

In all studies, the NanoSIMS images were corrected for electron multiplier dead time (44 ns) and applied dwell time (Table 2) by using the Look@NanoSIMS tool (Polerecky et al., 2012) for Matlab software (R2013b; The MathWorks, Inc., Natick, MA, USA).

As a preliminary step, regions of interest (ROI) were defined by thresholding using the Open MIMS Image plugin in the ImageJ software (Schneider et al., 2012). ROIs were defined based on the histogram distribution of $^{16}O^-$ for Study I, $^{12}C^{14}N^-$, $^{31}P^{16}O_2^-$ and $^{56}Fe^{16}O^-$ for Study II, and $^{12}C_2^-$ and $^{56}Fe^{16}O^-$ for Study III. According to the respective unimodal histogram distribution of the secondary ion images, the Huang (Huang and Wang, 1995) (Study I and III) or Triangle algorithm (Zack et al., 1977) (Study II) was used. The obtained thresholds for the NanoSIMS images were further used for ROI definition within the Look@NanoSIMS software.

In Study I, the goethite was characterized based on the $^{16}O^-$ to avoid a pre-differentiation between the goethite and a possibly formed Al oxide phase. The respective $^{27}Al^{16}O^-$ /$^{56}Fe^{16}O^-$ ratio of each pixel within the predefined ROI was calculated. Pixels statistically indicated as ‘outliers’ were reassigned to the NanoSIMS image by using the retained spatial information (Figure 4)

To visualize the spatial association of Fe oxides with SOM or phosphorus, the image analysis of Study I was further developed to create composite images that extend the pixel-wise information of Study I and enable the localization of congruent areas enriched in $^{12}C^{14}N^-$, $^{31}P^{16}O_2^-$ and $^{56}Fe^{16}O^-$. In Study II, the Fe oxides were characterized based on the $^{56}Fe^{16}O^-$ signal, while the SOM and phosphorus were characterized based on the $^{12}C^{14}N^-$ and $^{31}P^{16}O_2^-$ signal, respectively. To visualize the spatial association of Fe oxides with SOM or phosphorus, the ROIs were further processed by using a slightly adapted version of the R (R Core Team, 2018) code developed by Werner et al. (2017). Based on the known pixel size of the NanoSIMS images, it is possible to calculate the area of each ROI. As a result, it is possible to quantify the percentage of congruent areas, which can be considered as coverage of the Fe oxides with soil organic matter or phosphorus, respectively. Further, the $^{12}C^{14}N^-/^{56}Fe^{16}O^-$ and $^{31}P^{16}O_2^-/^{56}Fe^{16}O^-$ ratio was calculated for each ROI (Figure 5) to evaluate differences between the association of soil organic matter or phosphorus with Fe oxides formed at the Mn bar and synthetic Fe oxides at the Fe bar.

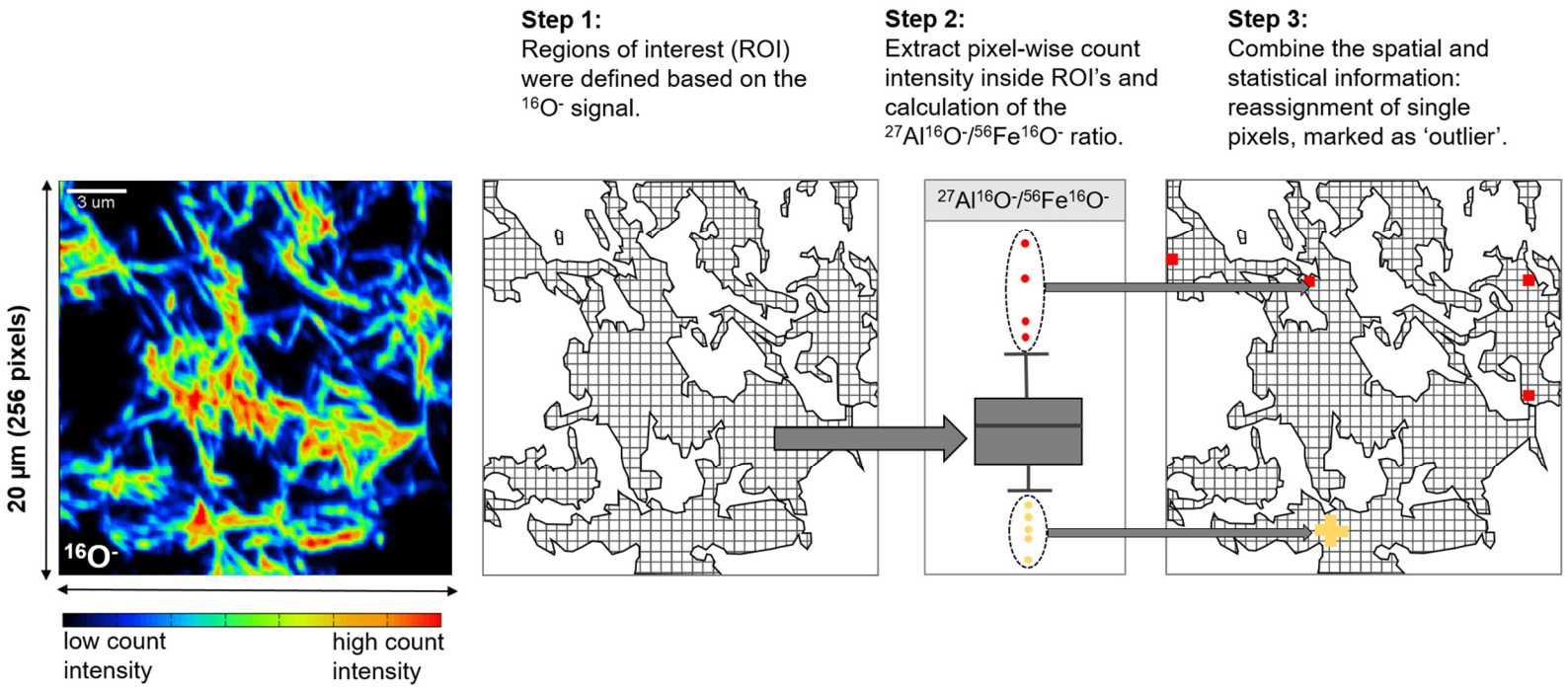

Figure 4: Schematic overview of the NanoSIMS image analysis developed for Study I, which enables the reassignment of single pixels statistically indicated as 'outliers' to their original localization within the NanoSIMS image (adapted from Pohl et al., 2018; Study I).

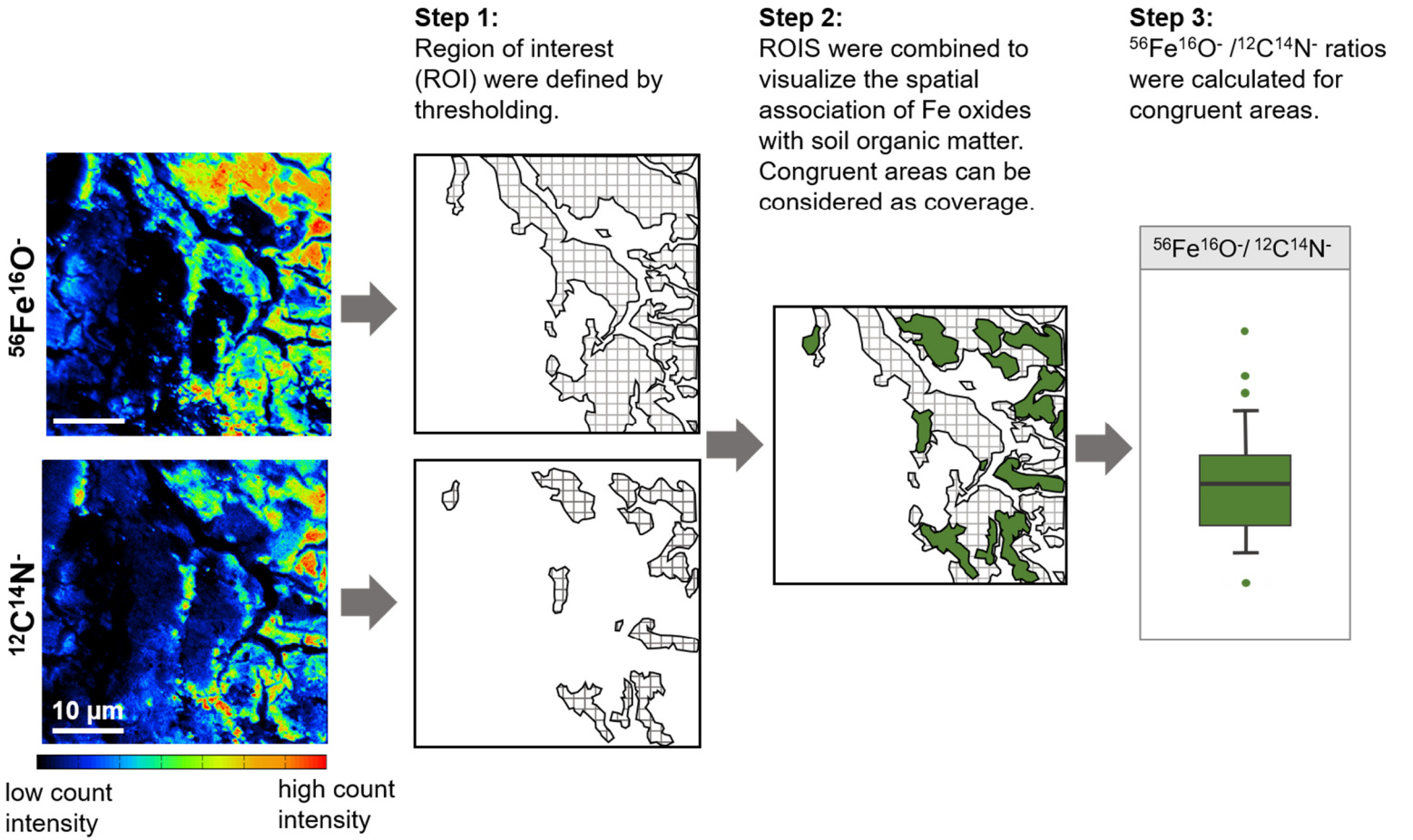

Figure 5: Schematic overview of the NanoSIMS image analysis developed for Study II, which extends the pixel-wise information of Study I. This enables the localization of congruent areas, which can be considered as coverage of the Fe oxides with, for example, soil organic matter. The $^{12}C^{14}N^-/^{56}Fe^{16}O^-$ ratio and, based on the known pixel size, the respective area can be calculated for each ROI separately.

In Study III, the use of the resin as embedding material adds an artificial C and N source to the sample. To differentiate between soil organic matter and resin, the $^{12}C^{14}N^-/^{12}C_2^-$ ratio was used. The $^{12}C^{14}N^-$ count intensity of the resin is lower than that of soil organic matter, which allows a clear distinction. The mean ratio $^{12}C^{14}N^-/^{12}C_2^-$ of the pure resin was calculated based on one NanoSIMS image (30 µm x 30 µm, 400 x 400 pixels), which was sectioned into 400 ROIs with a grid by using the Look@NanoSIMS software. To avoid the misclassification of resin as soil organic matter, the value of the highest outliner was used as a distinction threshold. The jarosite was characterized based on the $^{56}Fe^{16}O^-$ signal. To visualize the spatial association of soil organic matter and jarosite, the image analysis procedure developed in Study II was used to combine the predefined ROIs. In addition, ROIs with high $^{12}C_2^-$, but $^{56}Fe^{16}O^-$ count intensities beyond the threshold for jarosite were ascribed to the occurrence of small, resin-filled pores within the jarosite matrix. An integrated tool within the Look@NanoSIMS software allows the calculation of the diameter of a circle with the equivalent number of pixels within the respective ROIs. It can be assumed that the calculated diameter is equal to the pore size of the jarosite matrix. This enables the determination of pore size in embedded samples beyond the detection limit of µCT based only on NanoSIMS measurements.

3.4. Complementary imaging techniques

In Study II and Study III, complementary imaging techniques were used to support the interpretation of the data derived by NanoSIMS and to extend the analyzed sample area.

For Study II, hyperspectral imaging (HySpex) in the visible near-infrared (VNIR) was used to provide an overview of the redox bars and to capture the fine-scale spatial variance in spectral properties due to the occurrence of different Fe oxides (Viscarra Rossel et al., 2009; Viscarra Rossel et al., 2010). In total, an area of ~22 cm^2 of the Fe and Mn redox bars were analyzed before and after field installation. The camera (Norsk Elektro Optikk, Skedsmokorset, Norway) featured an automatic dark background correction, a moving translational stage, mounted spotlights to provide even illumination, and 1800 detectors, enabling a spatial resolution of 53 x 53 µm per pixel. The spectra were obtained over 186 bands in the region of 400 to 990 nm wavelength at a spectral resolution of 3.17 nm. Regions of contrasting variance were identified within the first three principal components. The data were averaged for each ROI, and another principal component analysis was applied to reveal

spectral relations and differences between the ROIs. The described analysis was performed by Christopher Just (Technical University of Munich).

For Study III, the embedded soil cores were analyzed prior to cutting with an X-ray microtomography (µCT, Zeiss Xradia Versa 520, Carl Zeiss Microscopy GmbH, Jena, Germany). The soil cores were scanned at a voltage of 80 keV and power of 7 W. A total of 1601 projections for each core were taken at an exposure time of 1 s with no filter. The 3D reconstruction was done by applying a beam hardening correction of 0.05 and achieved a field of view of 15 mm with a voxel edge size of 36 µm by which structures > 144 µm (4 voxels) could be confidently resolved. In one selected mangrove root core, a ROI was scanned with 4x magnification, resulting in a field of view of 8.57 mm and a voxel edge size of 5 µm. Image analysis of the reconstructed 3D datasets was done by the software MAVI (Modular Algorithms for Volume Images, Fraunhofer ITWM, Kaiserslautern) implemented in a Framework called ToolIP, where numerous 3D analytical solutions can be automatized using flow processing charts. Renderings were done with Paraview 5.4 (Kitware Inc., New York, USA). The grayscale images were filtered using a median filter with a window size of 33 voxels to reduce noise. Subsequent thresholds were selected by applying the Otsu (1979) algorithm to separate the grey values into single segments. To validate the segmentation, the median grey value for each area analyzed by NanoSIMS was calculated and co-registered with the corresponding µCT plane by a semi-automated registration plugin in ToolIP. The described analysis was performed by Daniel Uteau at the Department of Soil Science of the University of Kassel.

4. Results and Discussion

Chapter 4 only summarizes the results from the three studies performed for this doctoral thesis and will conclude with a separate overall discussion. A more detailed presentation of the results is available in the respective publication in the appendices.

4.1. Microscale spatial pattern of Al distribution in synthetic Fe oxides (Study I)

For Study I, three goethite samples with an increasing concentration of Al (0.1, 3, and 7%) were synthesized, and a linear correlation between the molar ratio derived by total digestion and the $^{27}Al^{16}O^{-}/^{56}Fe^{16}O^{-}$ ion ratio derived by NanoSIMS was verified. This demonstrates that the increasing Al concentration up to 7 % in synthetic goethite samples is reflected by a linear increasing $^{27}Al^{16}O^{-}/^{56}Fe^{16}O^{-}$ ion ratio.

The results were further compared with the commonly used method from Schulze (1984), which estimated the concentration of incorporated Al based on XRD analysis and the detectable shift to decreasing d-spacings with increasing concentration of Al. It was shown that the method from Schulze (1984) overestimates the concentration of incorporated Al, in particular at low Al concentrations. For example, in the sample with the lowest substitution grade, a concentration of 1.4 % was calculated, while with total digestion, only 0.1% Al was detectable. In contrast, the NanoSIMS analyses reflect the low molar ratios with a low $^{27}Al^{16}O^{-}$ count intensity and a small $^{27}Al^{16}O^{-}/^{56}Fe^{16}O^{-}$ ion ratio.

Besides the characteristic goethite peaks, the XRD analysis of the sample with the highest Al-substitution (7%) exhibited additional peaks of hematite (Fe_2O_3). The formation of hematite is a by-product of the synthesis at high temperature and high concentration of Al, which favor its formation instead of goethite (Lewis and Schwertmann, 1979; Schwertmann et al., 2000a). The XRD and FTIR analysis demonstrated that the respective peak positions were in agreement with reported values for pure, non-substituted hematite. Al can also be incorporated into hematite, but the concentration in goethite always exceeds the concentration in hematite under natural and synthetic conditions by about twice (Schulze and Schwertmann, 1987; Schwertmann and Kämpf, 1985). Consequently, it can be assumed that the formed hematite is depleted in Al in comparison to goethite. To investigate whether the different Al concentrations were also reflected in the NanoSIMS analysis, the

images were analyzed pixel by pixel. The goethite was characterized based on the histogram distribution of $^{16}O^-$. The pixel-wise analysis of the NanoSIMS images from the sample with the highest Al-substitution (7%) showed that the variability of the single-pixel ratios was very small. Only 1.1% of all pixels within the predefined ROIs had a significantly lower $^{27}Al^{16}O^-/^{56}Fe^{16}O^-$ ratio and were statistically characterized as 'outliers'. However, these 'outliers' were reassigned to the position within the original image and revealed spot-wise clusters with statistically lower $^{27}Al^{16}O^-/^{56}Fe^{16}O^-$ ratios. In contrast, the analysis of the statistical outliers defined in the NanoSIMS of the lower Al concentration levels (0.1% and 3%) showed no similar spatial pattern. Consequently, the round-shaped clusters, which were depleted in Al and only detectable in this spatial pattern in the sample with the highest Al substitution, were interpreted as hematite.

In summary, Study I demonstrated that the concentration of incorporated Al in synthetic goethite can be depicted by using NanoSIMS. Differences in ionization efficiency, which may be caused as a consequence of the different crystallinity of the sample matrix (Gabitov et al., 2013), could not be noted and had no effect on the linear correlation between the total Al content and the $^{27}Al^{16}O^-/^{56}Fe^{16}O^-$ ratio. In addition, based on the statistical evaluation of the individual pixels and the spatial reassignment within the NanoSIMS image, spatial patterns that can be ascribed to different Fe oxides were recognizable.

4.2. Spatial distribution of phosphorus and SOM as a function of the formation conditions of Fe oxides (Study II)

In Study II, redox bars coated with Fe and Mn oxides were installed for 30 days in a Mollic Gleysol. A section from the redox bar surface (3 x 3 mm, at 20 cm soil depth) was used for further analysis. The mean water table depth during the installation period was at 28 cm below and oscillated between 22 and 38 cm. Consequently, the measurement spots for the NanoSIMS measurements were within the capillary fringe.

The XRD results of the redox bar material after field installation suggested that the mineralogical composition of the synthetic Fe oxides is dominated by the initially applied goethite, while the originally applied ferrihydrite was not detectable. However, poorly crystalline ferrihydrite is often hard to identify by XRD (Childs, 1992) and might still be attached to the sample surface even though the characteristic peaks were not present in the XRD pattern. Probably for this reason,

the natural Fe oxides formed along the Mn bar could also not be identified by XRD, even though they were macroscopically detectable. However, the VNIR spectra reveal a small spectral overlap due to similar properties from naturally formed Fe oxides and the synthetic Fe oxide coating. Therefore, even without distinct mineralogical characterization, the formation of Fe oxides at the surface could be proven. It can be assumed that the naturally formed oxides are mainly poorly crystalline Fe oxides. The formation was influenced by the high concentration of dissolved OC reported for the study site (Mansfeldt and Overesch, 2013), which can inhibit crystal growth (Schwertmann et al., 2005) and increase the short-range ordered character of the resulting Fe mineral.

To visualize the spatial association of the natural and synthetic Fe oxides with SOM or phosphorus, the image analysis of Study I was further developed to create composite images. These images extend the pixel-wise information of Study I and enable the localization of congruent areas enriched in $^{12}C^{14}N^-$, $^{31}P^{16}O_2^-$, and $^{56}Fe^{16}O^-$. ROIs were determined based on the histogram distribution of $^{56}Fe^{16}O^-$ to define the Fe oxides within the NanoSIMS images. The percentage of the congruent area with $^{12}C^{14}N^-$ and $^{31}P^{16}O_2^-$ can be considered as coverage of the Fe oxides with SOM or phosphorus, respectively. Even though the redox bars were installed only for the relatively short period of 30 days, a mean coverage of 71 ± 25 % for $^{12}C^{14}N^-$ and 68 ± 33 % for $^{31}P^{16}O_2^-$ was found for the natural Fe oxides, while the mean coverage of the synthetic Fe oxides was lower with 43 ± 28 % for $^{12}C^{14}N^-$ and 47 ± 35 % for $^{31}P^{16}O_2^-$.

The analysis revealed that within the predefined ROIs, the spatial allocation of $^{12}C^{14}N^-$ and $^{31}P^{16}O_2^-$ matched almost congruently for synthetic and natural Fe oxides. There are almost no pixels where $^{12}C^{14}N^-$ and $^{31}P^{16}O_2^-$ can be detected separately from each other. For this reason, the calculated coverage values of $^{12}C^{14}N^-$ and $^{31}P^{16}O_2^-$ are almost identical for the natural and the synthetic Fe oxides, respectively. The respective $^{56}Fe^{16}O^-/^{12}C^{14}N^-$ and $^{56}Fe^{16}O^-/^{31}P^{16}O_2^-$ mean ratios of the ROIs were smaller for the natural in comparison to the synthetic Fe oxides, provoked by a higher count intensity of $^{12}C^{14}N^-$ and $^{31}P^{16}O_2^-$. This finding is in line with other studies, which described a higher loading of SOM or phosphate for less crystalline in comparison to more crystalline Fe oxides (Eusterhues et al., 2005; Mikutta et al., 2006; Parfitt, 1989). In addition, the natural Fe oxides were formed in the presence of the soil solution, which leads to coprecipitation with SOM and might have yielded higher C-loadings (Eusterhues et al., 2011) for the natural in comparison to the synthetic Fe oxides.

Study II demonstrated that the different mineralogical properties of synthetic and natural Fe oxides directly influence the extent of phosphorus and SOM coverage at the microscale under in-situ conditions. Mansfeldt et al. (2012) demonstrated, by using Mössbauer spectroscopy, that nanogoethite and ferrihydrite were the most dominant Fe phases in a study site adjacent to the site where the redox bars were installed. This confirms the importance of less crystalline Fe minerals for nutrient cycling in soils under changing redox conditions. In particular, less crystalline Fe oxides are preferentially microbial reduced under anaerobic conditions (Roden, 2003), while increasing C-loading of Fe oxides can lead to an increased (Shimizu et al., 2013) or decreased (Eusterhues et al., 2014) reduction rate, depending on microbial community composition. As demonstrated in Study II, the combination of redox bars, IRIS, and NanoSIMS is suitable to study the stability and distribution of poorly crystalline Fe oxides under naturally varying redoximorphic conditions and can thus contribute to understand the processes that lead to carbon (de)stabilization in redoximorphic soils. By using the developed image analysis, it is possible to determine the spatial association of Fe oxides with, for example, SOM or phosphorus while taking the temporal formation conditions into account at the same time. Even though only Fe oxides from one soil depth were examined for the analysis, the length of the redox bars (approx. 60 cm) allows different redox conditions that occur across the soil profile to be identified and integrated into the interpretation.

4.3. Spatial distribution of SOM in jarositic phyto tubules as a function of the microporosity (Study III)

In Study III, resin-embedded jarositic phyto tubules (i.e., preserved root fragments enclosed by tubular accumulations of jarosite) (Brewer and Sleeman, 1988) from a drained Salic Fluvisol (Hyperthionic, Drainic) (IUSS Working Group WRB, 2014) were investigated by using a combination of µCT, light microscopy, EDX-SEM, and NanoSIMS.

By using µCT, the investigated jarositic phyto tubule could be differentiated into two distinct zones with either high or low jarosite concentration at distances of < 0.5 mm and 0.5 - 1.9 mm from the relict root channel in the center, respectively. The two zones could be distinguished based on the grey value distribution of the µCT scans. The grey value depends on the X-ray density (i.e., linear attenuation coefficient) and is influenced by the density and atomic number of the material (Ketcham, 2005). Therefore, jarosite appeared brighter within the µCT scan, while less dense

constituents like the resin showed darker grey values. With increasing distance from the root channel, the median grey value changed from brighter to darker grey, indicating a change in the jarosite density and a greater contribution of the resin regarding the median grey value. Concomitantly, the volumetric percentage of the jarosite-enriched matrix decreased from a maximum of 32.6 % v/v at a distance from 0.5 mm to almost 0 % at 1.9 mm from the relict root channel. In addition, the total visible porosity (pores > 20 µm) increased from 0 in close vicinity to the root channel to 25.3 vol.-% in the outer margin of the soil core. The two zones could also be clearly distinguished in the light microscope image by a change of color from dark orange to pale yellow with increasing distance from the relict root channel. The EDX -SEM results show that the change in color is not caused by the incorporation of different elements, which may occur in jarosite (e.g., Na, Pb, Al, As, see e.g., Desborough et al., 2010).

To visualize the SOM distribution depending on the jarosite distribution within the two distinct zones, the image analysis investigated in Study II was further developed. The use of the resin as embedding material adds an artificial C and N source to the sample. However, the $^{12}C^{14}N^-$ count intensity of the resin is lower than that of SOM. Therefore, by calculating the mean ratio $^{12}C^{14}N^-/^{12}C_2^-$ of the pure resin, the value can be used as an additional threshold in the image analysis to clearly differentiate between resin and SOM (see chapter 3.3.2). It could be shown that in the zone with a high jarosite concentration, 85 ± 23 % of the jarosite was associated with SOM, while in the zone with a low jarosite concentration, only 32 ± 31 % was associated. This implies a higher concentration of SOM in close vicinity to the relict root channel. In the zone with high jarosite concentration, the SOM was detectable in single, isolated pores with a size of 525 ± 496 nm, whereby the diameter of the majority of the pores was in the size range between 200 and 400 nm (median value: 370 nm). If hydrologic conditions change and the soil would be re-flooded, e.g., for remediation purposes (Creeper et al., 2015a; Johnston et al., 2014; Kölbl et al., 2019; Wong et al., 2016), the SOM occurring in the zone with high jarosite concentration would be a potential carbon source for sulfate-reducing bacteria. However, most of the known sulfate-reducing bacteria have a cell size of 200 – 800 nm (Luan et al., 2020) and are thus partially larger than the majority of the pores in the zone with high jarosite concentration. In contrast, in the zone with low jarosite concentration, the pore size would be sufficient for microbial access, but the OC co-occurred almost exclusively with jarosite, which can hamper microbial degradation (Kleber et al., 2015).

The results clearly demonstrate the advantage of NanoSIMS in comparison to classical bulk methods. Bulk measurements only showed that the OC concentration of the jarositic phyto tubules (4.21 ± 0.65 mg g^{-1}) was higher than in the bulk soil (2.94 ± 0.13 mg g^{-1}), while the implementation of the developed image analysis revealed the heterogeneous OC distribution within the jarositic phyto tubules, as well as the limited spatial accessibility to microbes. Accordingly, results from Study III demonstrated that spatial accessibility needs to be considered for the design of potential remediation concepts, and bulk concentration is not sufficient as the sole information on carbon availability.

4.4. Spatial distribution of SOM and phosphorus in Fe oxide concretions and nodules as a function of the microscale properties (Study I, II, and III)

If redox concentrations are cemented over time in redoximorphic soils, they are defined as nodules or concretions. Concretions are characterized by an internal concentric structure as a result of fluctuating redox conditions, which lead to periodic precipitation and dissolution of minerals (Zhang and Karathanasis, 1997). Nodules, in contrast, exhibit no distinct layers (Schoeneberger et al., 2012). In the past, a large number of studies investigated the chemical and (micro-)morphological properties of redox concentrations (e.g., Cescas et al., 1970; Childs, 1975; Gallaher et al., 1973). They were demonstrated to be enriched in phosphorus and OC (e.g., Abekoe and Tiessen, 1998; Bird et al., 1994; Gasparatos et al., 2019; Schwertmann and Fanning, 1976) and thus play a critical role in the dynamic nutrient availability in redoximorphic soils. Redox concentrations often consist of a mixture of Fe oxides (e.g., goethite and ferrihydrite) and Mn oxides (e.g., birnessite) (summarized in Gasparatos et al., 2019). The concentric internal microstructure of redox concentrations (Ettler et al., 2017; Yu and Lu, 2016) may therefore be accompanied by different mineral properties regarding the adsorption and concomitant stabilization of, for example, OC and phosphorus. However, little is known about the distribution of OC and phosphorus as a function of the spatial distribution of the mineral phases.

In Study III, jarositic redox concentrations from a Salic Fluvisol (Hyperthionic, Drainic) (IUSS Working Group WRB, 2014) were investigated. Here, the redox concentrations have formed due to the draining of the area (Fitzpatrick et al., 2012) and the associated oxidation of the contained pyrite. Even if the formation conditions differ considerably from soils that are classically considered to be redoximorphic

(e.g., Gleysols or Stagnosols), Study III demonstrated that NanoSIMS could provide crucial information about the spatial accessibility of OC and thus contribute to understand the processes that lead to the long-term carbon stabilization within redox concentrations (Elberling et al., 2013). As demonstrated in Study II, the different sorption properties of (poorly) crystalline Fe oxides, such as goethite and ferrihydrite, can be reflected by NanoSIMS by exhibiting distinct coverage values. Although Study II focused exclusively on the analysis of Fe oxides, combined analyses of Mn and Fe oxides with NanoSIMS are feasible and have been performed in the past (Peng et al., 2015; Rennert et al., 2014). If combined with the results of Study I and the image analysis protocol developed in Study II, the interpretation could additionally include the influence of cations incorporated in the mineral structure. Study I demonstrated that the Fe/Al ratio in Fe oxides can be measured by NanoSIMS. Thus, it would be possible, for example, to study the effect of the Al substitution within redox concentrations with respect to the spatial distribution of OC and phosphorus. In bulk adsorption experiments, it was already shown that the adsorption of phosphate increases with increasing substitution of Al in goethite (Hsu et al., 2020; Li et al., 2019). NanoSIMS is one of the few techniques able to analyze the Fe/Al ratio of Fe oxides within the soil structure and within different layers of individual concretions and to prove whether Al-substitution has a strong influence on SOM adsorption. Even though only Al was considered in Study I, goethite, as well as other Fe oxides, can incorporate more elements within their mineral structure (e.g., Cu or Ni, see e.g., Cornell and Schwertmann, 2003). As a result, increased concentrations of heavy metals can also occur in redox concentrations (Ettler et al., 2017; Yu and Lu, 2016). Since NanoSIMS can also be used to measure other metals, such as Cu and Ni (Du et al., 2018; Smart et al., 2007), the presumed periodic incorporation of other metals could be studied. Consequently, high spatial resolution analyses, like NanoSIMS, make it feasible to assess the interplay of oxide formation and dissolution, as well as to address the associated accumulation or release of nutrients (like, e.g., P or SOM), but also of pollutants like heavy metals.

5. Conclusions

This thesis investigated spatial patterns of elemental distributions of Fe minerals in redoximorphic soils by developing an analysis protocol for NanoSIMS images. This approach enabled qualitative and quantitative conclusions about the microscale properties of typical synthetic (Study I) and natural (Study II and III) soil minerals.

Two of the studies demonstrated the effectiveness of NanoSIMS in visualizing and quantifying the heterogeneous distribution of SOM (Studies II and III) and phosphorus (Study II) across different underlying mineral phases at the microscale and provided direct evidence for the importance of Fe minerals in the stabilization and distribution of SOM in active (Study II) and relict redoximorphic (Study III) soils.

In Study II, it was shown that poorly crystalline natural Fe oxides, which have formed within only 30 days in a redoximorphic soil, have a higher degree of coverage of SOM and phosphorus than well-crystalline, synthetic Fe oxides introduced into the soil. The quantitative image analysis revealed that the natural Fe oxides exhibited nearly twice the SOM ($^{12}C^{14}N^-$) and P ($^{31}P^{16}O_2^-$) coverage than the synthetic Fe oxides. We assume that this difference can be explained by a higher adsorption capacity due to a lower crystallinity of the natural Fe oxides.

In Study II, we assumed that the low crystallinity was caused by the high concentration of dissolved OC reported for the study site. However, the crystallinity of Fe oxides can also be influenced by the incorporation of a wide range of cations. Study I focused on the analysis of Al as the most commonly observed substituent of Fe^{III}. The results demonstrated that NanoSIMS can accurately estimate the concentration of incorporated Al based on the $^{27}Al^{16}O^-/^{56}Fe^{16}O^-$ ion ratio. This means that not only the spatial distribution of Al but also the concentrations derived from the $^{27}Al^{16}O^-/^{56}Fe^{16}O^-$ ion ratio can be included in the interpretation of the NanoSIMS images. In study I, we also took advantage of the fact that hematite incorporates less Al than goethite (Schulze and Schwertmann, 1987; Schwertmann and Kämpf, 1985). In combination with XRD, it was thus possible to spatially distinguish goethite from hematite crystals.

In Study III, the statistical evaluation of the $^{12}C^{14}N^-/^{12}C_2^-$ ion ratio allowed the clear differentiation between SOM and the embedding resin of the thin sections. As a result, it was shown that carbon is not only associated with the mineral phase but is additionally entrapped in micropores. Image analysis revealed that the diameter of the majority of the pores is below the size of most microorganisms. We conclude that microbial accessibility is hampered and that the entrapped SOM might

contribute to the described long-term carbon stabilization within redox concentrations.

Overall, the three studies demonstrated that NanoSIMS, in combination with the appropriate image analysis, is a valuable complement to conventional methods to understand the functioning of Fe minerals in redoximorphic soils. The developed image analysis protocol enables the identification and quantification of spatial patterns, the assessment of associations between various elements, and the investigation of the influence of mineralogical properties on the distribution of, for example, SOM. These findings contribute to advancing our knowledge of the complex processes occurring at the microscale in soil systems and can thus provide insights into the Fe mineral stability and dynamic in redoximorphic soils.

References

Abekoe, M.K., Tiessen, H., 1998. Phosphorus forms, lateritic nodules and soil properties along a hillslope in northern Ghana. Catena 33 (1), 1–15.

AG Boden, 2005. Bodenkundliche Kartieranleitung. KA5, 5. Auflage ed. Schweizerbart Science Publishers, Stuttgart, Hannover, 438 pp.

Ainsworth, C.C., Sumner, M.E., 1985. Effect of Aluminum Substitution in Goethite on Phosphorus Adsorption: II. Rate of Adsorption. Soil Sci. Soc. Am. J. 49 (5), 1149–1153.

Alongi, D.M., Wattayakorn, G., Pfitzner, J., Tirendi, F., Zagorskis, I., Brunskill, G.J., Davidson, A., Clough, B.F., 2001. Organic carbon accumulation and metabolic pathways in sediments of mangrove forests in southern Thailand. Mar. Geol. 179 (1-2), 85–103.

Alvarez, M., Tufo, A.E., Zenobi, C., Ramos, C.P., Sileo, E.E., 2015. Chemical, structural and hyperfine characterization of goethites with simultaneous incorporation of manganese, cobalt and aluminum ions. Chem. Geol. 414 (4), 16–27.

Anthony, T.L., Silver, W.L., 2020. Mineralogical associations with soil carbon in managed wetland soils. Glob. Chang. Biol. 26 (11), 6555–6567.

Baldock, J.A., Skjemstad, J.O., 2000. Role of the soil matrix and minerals in protecting natural organic materials against biological attack. Org. Geochem. 31 (7-8), 697–710.

Baveye, P.C., Otten, W., Kravchenko, A., Balseiro-Romero, M., Beckers, É., Chalhoub, M., Darnault, C., Eickhorst, T., Garnier, P., Hapca, S., Kiranyaz, S., Monga, O., Mueller, C.W., Nunan, N., Pot, V., Schlüter, S., Schmidt, H., Vogel, H.-J., 2018. Emergent Properties of Microbial Activity in Heterogeneous Soil Microenvironments: Different Research Approaches Are Slowly Converging, Yet Major Challenges Remain. Front. Microbiol. 9, 1929.

Bigham, J.M., Fitzpatrick, R.W., Schulze, D.G., 2002. Iron Oxides, in: Dixon, J.B., Schulze, D.G. (Eds.), Soil Mineralogy with Environmental Applications. SSSA Book Series: 7. Soil Science Society of America, Madison, WI, USA, pp. 323–366.

Bird, M.I., Quade, J., Chivas, A.R., Fifield, L.K., Allan, G.L., Head, M.J., 1994. The carbon isotope composition of organic matter occluded in iron nodules. Chem. Geol. 114 (3-4), 269–279.

Borch, T., Fendorf, S., 2007. Phosphate Interactions with Iron (Hydr)oxides: Mineralization Pathways and Phosphorus Retention upon Bioreduction: Chapter 12, in: Barnett, M.O., Kent, D.B. (Eds.), Adsorption of Metals by Geomedia II. Variables, Mechanisms, and Model Applications, vol. 7. Developments in Earth and Environmental Sciences. Elsevier, Amsterdam, The Netherlands, pp. 321–348.

Brewer, R., Sleeman, J.R., 1988. Soil Structure and Fabric. CSIRO Publishing, Adelaide, Australia.

Cescas, M.P., Tyner, E.H., Harmer, R.S., 1970. Ferromanganiferous Soil Concretions: A Scanning Electron Microscope Study of Their Micropore Structures. Soil Sci. Soc. Am. J. 34 (4), 641–644.

Chen, C., Hall, S.J., Coward, E., Thompson, A., 2020. Iron-mediated organic matter decomposition in humid soils can counteract protection. Nat. Commun. 11 (1), 2255.

Childs, C.W., 1975. Composition of iron-manganese concretions from some New Zealand soils. Geoderma 13 (2), 141–152.

Childs, C.W., 1992. Ferrihydrite: A review of structure, properties and occurrence in relation to soils. Z. Pflanzenernaehr. Bodenk. 155 (5), 441–448.

Coby, A.J., Picardal, F., Shelobolina, E., Xu, H., Roden, E.E., 2011. Repeated anaerobic microbial redox cycling of iron. Appl. Environ. Microbiol. 77 (17), 6036–6042.

Cornell, R.M., Schwertmann, U., 2003. The Iron Oxides: Structure, Properties, Reactions, Occurences and Uses, 2nd ed. Wiley-VCH, Weinheim, 664 pp.

Creeper, N.L., Hicks, W.S., Shand, P., Fitzpatrick, R.W., 2015a. Geochemical processes following freshwater reflooding of acidified inland acid sulfate soils: An in situ mesocosm experiment. Chem. Geol. 411, 200–214.

Creeper, N.L., Shand, P., Hicks, W., Fitzpatrick, R.W., 2015b. Porewater geochemistry of inland Acid sulfate soils with sulfuric horizons following postdrought reflooding with freshwater. J. Environ. Qual. 44 (3), 989–1000.

Desborough, G.A., Smith, K.S., Lowers, H.A., Swayze, G.A., Hammarstrom, J.M., Diehl, S.F., Leinz, R.W., Driscoll, R.L., 2010. Mineralogical and chemical characteristics of some natural jarosites. Geochim. Cosmochim. Acta 74 (3), 1041–1056.

Dorau, K., Eickmeier, M., Mansfeldt, T., 2016. Comparison of Manganese and Iron Oxide-Coated Redox Bars for Characterization of the Redox Status in Wetland Soils. Wetlands 36 (1), 133–141.

Dorau, K., Mansfeldt, T., 2015. Manganese-oxide-coated redox bars as an indicator of reducing conditions in soils. J. Environ. Qual. 44 (2), 696–703.

Dorau, K., Mansfeldt, T., 2016. Manganese and iron oxide-coated redox bars as a tool to in situ study the element sorption in wet soils. J. Soils Sediments 16 (3), 976–986.

Dorau, K., Pohl, L., Just, C., Höschen, C., Ufer, K., Mansfeldt, T., Mueller, C.W., 2019. Soil Organic Matter and Phosphate Sorption on Natural and Synthetic Fe Oxides under in Situ Conditions. Environmental science & technology 53 (22), 13081–13087.

Dorau, K., Wessel-Bothe, S., Milbert, G., Schrey, H.P., Elhaus, D., Mansfeldt, T., 2020. Climate change and redoximorphosis in a soil with stagnic properties. Catena 190, 104528.

Du, H., Huang, Q., Zhou, M., Tie, B., Lei, M., Wei, X., Liu, X., Yang, Y., 2018. Sorption of Cu(II) by Al hydroxide organo–mineral coprecipitates: Microcalorimetry and NanoSIMS observations. Chem. Geol. 499 (5), 165–171.

Elberling, B., Breuning-Madsen, H., Knicker, H., 2013. Carbon sequestration in iron-nodules in moist semi-deciduous tropical forest soil. Geoderma 200-201 (2), 202–207.

Ettler, V., Chren, M., Mihaljevič, M., Drahota, P., Kříbek, B., Veselovský, F., Sracek, O., Vaněk, A., Penížek, V., Komárek, M., Mapani, B., Kamona, F., 2017. Characterization of Fe-Mn concentric nodules from Luvisol irrigated by mine water in a semi-arid agricultural area. Geoderma 299, 32–42.

Eusterhues, K., Hädrich, A., Neidhardt, J., Küsel, K., Keller, T.F., Jandt, K.D., Totsche, K.U., 2014. Reduction of ferrihydrite with adsorbed and coprecipitated organic matter: microbial reduction by Geobacter bremensis vs. abiotic reduction by Na-dithionite. Biogeosciences 11 (18), 4953–4966.

Eusterhues, K., Rennert, T., Knicker, H., Kögel-Knabner, I., Totsche, K.U., Schwertmann, U., 2011. Fractionation of organic matter due to reaction with ferrihydrite: coprecipitation versus adsorption. Environ. Sci. Technol. 45 (2), 527–533.

Eusterhues, K., Rumpel, C., Kleber, M., Kögel-Knabner, I., 2003. Stabilisation of soil organic matter by interactions with minerals as revealed by mineral dissolution and oxidative degradation. Org. Geochem. 34 (12), 1591–1600.

Eusterhues, K., Rumpel, C., Kögel-Knabner, I., 2005. Organo-mineral associations in sandy acid forest soils: importance of specific surface area, iron oxides and micropores. Eur. J. Soil Science 56, 753-763.

Fältmarsch, R.M., Åström, M.E., Vuori, K.-M., 2008. Environmental risks of metals mobilised from acid sulphate soils in Finland: a literature review. Boreal Env. Res. 13 (5), 444–456.

Ferreira, T.O., Otero, X.L., Vidal-Torrado, P., Macías, F., 2007. Effects of bioturbation by root and crab activity on iron and sulfur biogeochemistry in mangrove substrate. Geoderma 142 (1-2), 36–46.

Fisher, B.J., Faust, J.C., Moore, O.W., Peacock, C.L., März, C., 2021. Technical note: Uncovering the influence of methodological variations on the extractability of iron-bound organic carbon. Biogeosciences 18 (11), 3409–3419.

Fitzpatrick, R.W., Schwertmann, U., 1982. Al-substituted goethite - an indicator of pedogenic and other weathering environments in South Africa. Geoderma (27), 335–347.

Fitzpatrick, R.W., Thomas, B., Merry, R., Marvanek, S., 2012. A field guide to estuarine soil-landscapes in Barker Inlet, South Australia. Acid Sulfate Soils Centre (ASSC), Adelaide, Australia.

Gabitov, R.I., Gagnon, A.C., Guan, Y., Eiler, J.M., Adkins, J.F., 2013. Accurate Mg/Ca, Sr/Ca, and Ba/Ca ratio measurements in carbonates by SIMS and NanoSIMS and an assessment of heterogeneity in common calcium carbonate standards. Chem. Geol. 356 (5070), 94–108.

Gallaher, R.N., Perkins, H.F., Radcliffe, D., 1973. Soil Concretions: I. X-Ray Spectrograph and Electron Microprobe Analyses. Soil Sci. Soc. Am. J. 37 (3), 465–469.

Gasparatos, D., Massas, I., Godelitsas, A., 2019. Fe-Mn concretions and nodules formation in redoximorphic soils and their role on soil phosphorus dynamics: Current knowledge and gaps. Catena 182, 104106.

Greenberg, W.A., Wilding, L.P., 1998. Evidence for Contemporary and Relict Redoximorphic Features of an Alfisol in East-Central Texas, in: Rabenhorst, M.C., Bell, J.C., McDaniel, P.A. (Eds.), Quantifying Soil Hydromorphology. Volume 54, vol. 112. Soil Science Society of America, Madison, WI, USA, pp. 227–246.

Händel, M., Rennert, T., Totsche, K.U., 2013. A simple method to synthesize birnessite at ambient pressure and temperature. Geoderma 193-194 (4), 117–121.

Hansel, C.M., Lentini, C.J., Tang, Y., Johnston, D.T., Wankel, S.D., Jardine, P.M., 2015. Dominance of sulfur-fueled iron oxide reduction in low-sulfate freshwater sediments. ISME J. 9 (11), 2400–2412.

Hatton, P.-J., Remusat, L., Zeller, B., Derrien, D., 2012. A multi-scale approach to determine accurate elemental and isotopic ratios by nano-scale secondary ion mass spectrometry imaging. Rapid Commun. Mass Spectrom. 26 (11), 1363–1371.

Herrmann, A.M., Ritz, K., Nunan, N., Clode, P.L., Pett-Ridge, J., Kilburn, M.R., Murphy, D.V., O'Donnell, A.G., Stockdale, E.A., 2007. Nano-scale secondary ion mass spectrometry — A new analytical tool in biogeochemistry and soil ecology: A review article. Soil Biol. Biochem. 39 (8), 1835–1850.

Holmer, M., Kristensen, E., Banta, G., Hansen, K., Jensen, M., Bussawarit, N., 1994. Biogeochemical cycling of sulfur and iron in sediments of a south-east Asian mangrove, Phuket Island, Thailand. Biogeochemistry 26 (3), 145–161.

Hsu, L.-C., Tzou, Y.-M., Ho, M.-S., Sivakumar, C., Cho, Y.-L., Li, W.-H., Chiang, P.-N., Teah, H.Y., Liu, Y.-T., 2020. Preferential phosphate sorption and Al substitution on goethite. Environ. Sci.: Nano 7 (11), 3497–3508.

Huang, L.-K., Wang, M.-J.J., 1995. Image thresholding by minimizing the measures of fuzziness. Pattern Recognit. 28 (1), 41–51.

Inglett, P.W., Reddy, K.R., Corstanje, R., 2005. ANAEROBIC SOILS, in: Hillel, D. (Ed.), Encyclopedia of Soils in the Environment, vol. 46. Elsevier, Amsterdam, pp. 72–78.

Isbell, R., National Committee on Soil and Terrain, 2016. The Australian Soil Classification, 2nd ed. Australian Soil and Land Survey Handbook. CSIRO Publishing, Melbourne, Australia, 1152 pp.

IUSS Working Group WRB, 2015. World reference base for soil resources 2014: International soil classification system for naming soils and creating legends for soil maps. World Soil Resources Reports No. 106. FAO, Rome.

Jenkinson, B.J., Franzmeier, D.P., 2006. Development and Evaluation of Iron-Coated Tubes that Indicate Reduction in Soils. Soil Sci. Soc. Am. J. 70 (1), 183–191.

Johnston, S.G., Burton, E.D., Aaso, T., Tuckerman, G., 2014. Sulfur, iron and carbon cycling following hydrological restoration of acidic freshwater wetlands. Chem. Geol. 371, 9–26.

Johnston, S.G., Keene, A.F., Bush, R.T., Burton, E.D., Sullivan, L.A., Smith, D., McElnea, A.E., Martens, M.A., Wilbraham, S., 2009. Contemporary pedogenesis of severely degraded tropical acid sulfate soils after introduction of regular tidal inundation. Geoderma 149 (3-4), 335–346.

Kaiser, K., Guggenberger, G., 2000. The role of DOM sorption to mineral surfaces in the preservation of organic matter in soils. Org. Geochem. 31 (7-8), 711–725.

Ketcham, R.A., 2005. Three-dimensional grain fabric measurements using high-resolution X-ray computed tomography. J. Struct. Geol. 27 (7), 1217–1228.

Kilburn, M.R., Wacey, D., 2015. Nanoscale Secondary Ion Mass Spectrometry (NanoSIMS) as an Analytical Tool in the Geosciences, in: Grice, K. (Ed.), Principles and practice of analytical techniques in geosciences 4. Royal Society of Chemistry, Cambridge, pp. 1–34.

Kleber, M., Eusterhues, K., Keiluweit, M., Mikutta, C., Mikutta, R., Nico, P.S., 2015. Mineral–Organic Associations: Formation, Properties, and Relevance in Soil Environments. Adv. Agron. 130, 1–140.

Kölbl, A., Bucka, F., Marschner, P., Schulz, S., Lueders, T., Kögel-Knabner, I., 2019. Consumption and alteration of different organic matter sources during remediation of a sandy sulfuric soil. Geoderma 347, 220–232.

Kravchenko, A.N., Guber, A.K., 2017. Soil pores and their contributions to soil carbon processes. Geoderma 287, 31–39.

Kukkadapu, R.K., Zachara, J.M., Fredrickson, J.K., Smith, S.C., Dohnalkova, A.C., Russell, C.K., 2003. Transformation of 2-line ferrihydrite to 6-line ferrihydrite under oxic and anoxic conditions. Am. Min. 88 (11-12), 1903–1914.

Kukkadapu, R.K., Zachara, J.M., Smith, S.C., Fredrickson, J.K., Liu, C., 2001. Dissimilatory bacterial reduction of Al-substituted goethite in subsurface sediments. Geochim. Cosmochim. Acta 65 (17), 2913–2924.

Lewis, D.G., Schwertmann, U., 1979. The Influence of Aluminium on the Formation of Iron Oxides. IV. The Influence of [Al], [OH], and Temperature. Clays Clay Miner. 27 (3), 195–200.

Li, M., Liu, H., Chen, T., Wei, L., Wang, C., Hu, W., Wang, H., 2019. The transformation of α-(Al, Fe)OOH in natural fire: Effect of Al substitution amount on fixation of phosphate. Chem. Geol. 524 (2), 368–382.

Lindbo, D.L., Stolt, M.H., Vepraskas, M.J., 2010. Redoximorphic Features: Chapter 8, in: Stoops, G., Marcelino, V., Mees, F. (Eds.), Interpretation of micromorphological features of soils and regoliths. Elsevier, Amsterdam, Oxford, pp. 129–147.

Luan, L., Jiang, Y., Cheng, M., Dini-Andreote, F., Sui, Y., Xu, Q., Geisen, S., Sun, B., 2020. Organism body size structures the soil microbial and nematode community assembly at a continental and global scale. Nat. Commun. 11 (1), 6406.

Mansfeldt, T., Overesch, M., 2013. Arsenic mobility and speciation in a gleysol with petrogleyic properties: a field and laboratory approach. J. Environ. Qual. 42 (4), 1130–1141.

Mansfeldt, T., Schuth, S., Häusler, W., Wagner, F.E., Kaufhold, S., Overesch, M., 2012. Iron oxide mineralogy and stable iron isotope composition in a Gleysol with petrogleyic properties. J. Soils Sediments 12 (1), 97–114.

McMahon, G., Saint-Cyr, H.F., Lechene, C., Unkefer, C.J., 2006. CN- secondary ions form by recombination as demonstrated using multi-isotope mass spectrometry of 13C- and 15N-labeled polyglycine. J. Am. Soc. Mass Spectrom. 17 (8), 1181–1187.

Michael, P.S., Fitzpatrick, R.W., Reid, R., 2015. The role of organic matter in ameliorating acid sulfate soils with sulfuric horizons. Geoderma 255-256, 42–49.

Mikutta, R., Kleber, M., Torn, M.S., Jahn, R., 2006. Stabilization of Soil Organic Matter: Association with Minerals or Chemical Recalcitrance? Biogeochemistry 77 (1), 25–56.

Moeslundi, L., Thamdrup, B., Barker Jrgensen, B., 1994. Sulfur and iron cycling in a coastal sediment: Radiotracer studies and seasonal dynamics. Biogeochemistry 27 (2), 129–152.

Mueller, C.W., Hoeschen, C., Steffens, M., Buddenbaum, H., Hinkel, K., Bockheim, J.G., Kao-Kniffin, J., 2017a. Microscale soil structures foster organic matter stabilization in permafrost soils. Geoderma 293, 44–53.

Mueller, C.W., Kölbl, A., Hoeschen, C., Hillion, F., Heister, K., Herrmann, A.M., Kögel-Knabner, I., 2012. Submicron scale imaging of soil organic matter dynamics using NanoSIMS – From single particles to intact aggregates. Org. Geochem. 42 (12), 1476–1488.

Mueller, C.W., Remusat, L., Rumpel, C., 2017b. Characterization of Biogeochemical Processes at the Microscale: Concepts and Applications of NanoSIMS. Chapter 8., in: Chabbi, A., Loescher, H.W. (Eds.), Terrestrial Ecosystem Research Infrastructures. Challenges and Opportunities. CRC Press, Boca Raton, pp. 193–212.

Mueller, C.W., Weber, P.K., Kilburn, M.R., Hoeschen, C., Kleber, M., Pett-Ridge, J., 2013. Advances in the Analysis of Biogeochemical Interfaces: NanoSIMS to Investigate Soil Microenvironments. Adv. Agron. 121, 1–46.

Neumann, R., Avelar, A.N., da Costa, G.M., 2014. Refinement of the isomorphic substitutions in goethite and hematite by the Rietveld method, and relevance to bauxite characterisation and processing. Miner. Eng. 55 (12), 80–86.

Noël, V., Marchand, C., Juillot, F., Ona-Nguema, G., Viollier, E., Marakovic, G., Olivi, L., Delbes, L., Gelebart, F., Morin, G., 2014. EXAFS analysis of iron cycling in mangrove sediments downstream a lateritized ultramafic watershed (Vavouto Bay, New Caledonia). Geochim. Cosmochim. Acta 136 (1–2), 211–228.

Otero, X.L., Ferreira, T.O., Huerta-Díaz, M.A., Partiti, C.S.M., Souza, V., Vidal-Torrado, P., Macías, F., 2009. Geochemistry of iron and manganese in soils and sediments of a mangrove system, Island of Pai Matos (Cananeia — SP, Brazil). Geoderma 148 (3-4), 318–335.

Parfitt, R.L., 1989. Phosphate reactions with natural allophane, ferrihydrite and goethite. J. Soil Sci. 40 (2), 359–369.

Peng, X., Ta, K., Chen, S., Zhang, L., Xu, H., 2015. Coexistence of Fe(II)- and Mn(II)-oxidizing bacteria govern the formation of deep sea umber deposits. Geochim. Cosmochim. Acta 169, 200–216.

Peretyazhko, T., Sposito, G., 2005. Iron(III) reduction and phosphorous solubilization in humid tropical forest soils. Geochim. Cosmochim. Acta 69 (14), 3643–3652.

Pett-Ridge, J., Weber, P.K., 2012. NanoSIP: NanoSIMS applications for microbial biology. Methods Mol. Biol. 881, 375–408.

Poch, R.M., Thomas, B.P., Fitzpatrick, R.W., Merry, R.H., 2009. Micromorphological evidence for mineral weathering pathways in a coastal acid sulfate soil sequence with Mediterranean-type climate, South Australia. Soil Res. 47 (4), 403–422.

Pohl, L., Kölbl, A., Uteau, D., Peth, S., Häusler, W., Mosley, L., Marschner, P., Fitzpatrick, R., Kögel-Knabner, I., 2021. Porosity and organic matter distribution in jarositic phyto tubules of sulfuric soils assessed by combined µCT and NanoSIMS analysis. Geoderma 399 (1–2), 115124.

Pohl, L., Kölbl, A., Werner, F., Mueller, C.W., Höschen, C., Häusler, W., Kögel-Knabner, I., 2018. Imaging of Al/Fe ratios in synthetic Al-goethite revealed by nanoscale secondary ion mass spectrometry. Rapid Commun. Mass Spectrom. 32 (8), 619–628.

Polerecky, L., Adam, B., Milucka, J., Musat, N., Vagner, T., Kuypers, M.M.M., 2012. Look@NanoSIMS--a tool for the analysis of nanoSIMS data in environmental microbiology. Environ. Microbiol. 14 (4), 1009–1023.

Possinger, A.R., Bailey, S.W., Inagaki, T.M., Kögel-Knabner, I., Dynes, J.J., Arthur, Z.A., Lehmann, J., 2020. Organo-mineral interactions and soil carbon mineralizability with variable saturation cycle frequency. Geoderma 375 (3–4), 114483.

Postma, D., 1993. The reactivity of iron oxides in sediments: A kinetic approach. Geochim. Cosmochim. Acta 57 (21-22), 5027–5034.

Rabenhorst, M.C., Burch, S.N., 2006. Synthetic Iron Oxides as an Indicator of Reduction in Soils (IRIS). Soil Sci. Soc. Am. J. 70 (4), 1227–1236.

Rabenhorst, M.C., Haering, K.C., 1989. Soil micromorphology of a chesapeake bay tidal marsh: Implications for sulfur accumulation. Soil Sci. 147 (5), 339–347.

Reddy, K.R., DeLaune, R.D., 2008. Biogeochemistry of Wetlands. CRC Press, Boca Raton.

Rennert, T., Händel, M., Höschen, C., Lugmeier, J., Steffens, M., Totsche, K.U., 2014. A NanoSIMS study on the distribution of soil organic matter, iron and manganese in a nodule from a Stagnosol. Eur. J. Soil Science 65 (5), 684–692.

Roden, E.E., 2003. Fe(III) Oxide Reactivity Toward Biological versus Chemical Reduction. Environ. Sci. Technol. 37 (7), 1319–1324.

Roychoudhury, A.N., Kostka, J.E., van Cappellen, P., 2003. Pyritization: a palaeoenvironmental and redox proxy reevaluated. Estuar. Coast. Shelf Sci. 57 (5-6), 1183–1193.

Schlüter, S., Leuther, F., Albrecht, L., Hoeschen, C., Kilian, R., Surey, R., Mikutta, R., Kaiser, K., Mueller, C.W., Vogel, H.-J., 2022. Microscale carbon distribution around pores and particulate organic matter varies with soil moisture regime. Nat. Commun. 13 (1), 2098.

Schneider, C.A., Rasband, W.S., Eliceiri, K.W., 2012. NIH Image to ImageJ: 25 years of image analysis. Nat. Methods 9 (7), 671–675.

Schoeneberger, P.J., Wysocki, D.A., Benham, E.C., Soil Survey Staff, 2012. Field Book for Describing and Sampling Soils, 3rd ed. National Soil Survey Center, Lincoln, NE.

Schulze, D.G., 1984. The Influence of Alumnium on Iron Oxides. VIII. Unit-Cell Dimensions of Al-Substituted Goethites and Estimation of Al from them. Clays Clay Miner. 32 (1), 36–44.

Schulze, D.G., Schwertmann, U., 1984. The Influence of Aluminium on iron oxides: X. Properties of Al-Substituted Goethites. Clays Clay Miner. (19), 521–539.

Schulze, D.G., Schwertmann, U., 1987. The influence of aluminium on iron oxides: XIII. Properties of goethites synthesised in 0.3 M KOH at 25°C. Clays Clay Miner. 22 (1), 83–92.

Schwertmann, U., 1964. Differenzierung der Eisenoxide des Bodens durch Extraktion mit Ammoniumoxalat-Lösung. Z. Pflanzenernaehr. Bodenk. 105 (3), 194–202.

Schwertmann, U., 1984. Aluminiumsubstitution in pedogenen Eisenoxiden - eine Übersicht. Z. Pflanzenernaehr. Bodenk. (147), 385–399.

Schwertmann, U., Cornell, R.M., 2000. Iron oxides in the laboratory: Preparation and characterization, 2nd ed. Wiley-VCH, Weinheim, New York.

Schwertmann, U., Fanning, D.S., 1976. Iron-Manganese Concretions in Hydrosequences of Soils in Loess in Bavaria. Soil Sci. Soc. Am. J. 40 (5), NP-NP.

Schwertmann, U., Friedl, J., Stanjek, H., Schulze, D.G., 2000a. The Effect of Al on Fe Oxides. XIX. Formation of Al-Substituted Hematite from Ferrihydrite at 25°C and pH 4 To 7. Clays Clay Miner. 48 (2), 159–172.

Schwertmann, U., Friedl, J., Stanjek, H., Schulze, D.G., 2000b. The effect of clay minerals on the formation of goethite and hematite from ferrihydrite after 16 years' ageing at 25°C and pH 4 – 7. Clay miner. 35 (4), 613–623.

Schwertmann, U., Kämpf, N., 1985. Properties of Goethite and Hematite in Kaolinitic Soils of Southern and Central Brazil. Soil Sci. 139 (4), 344–350.

Schwertmann, U., Wagner, F., Knicker, H., 2005. Ferrihydrite-Humic Associations. Soil Sci. Soc. Am. J. 69 (4), 1009–1015.

Shimizu, M., Zhou, J., Schröder, C., Obst, M., Kappler, A., Borch, T., 2013. Dissimilatory reduction and transformation of ferrihydrite-humic acid coprecipitates. Environ. Sci. Technol. 47 (23), 13375–13384.

Smart, K.E., Kilburn, M.R., Salter, C.J., Smith, J.A.C., Grovenor, C.R.M., 2007. NanoSIMS and EPMA analysis of nickel localisation in leaves of the hyperaccumulator plant Alyssum lesbiacum. Int. J. Mass Spectrom. 260 (2-3), 107–114.

Thomas, G.E., Strobel, B.W., 2022. Mobility of iron-oxide associated elements in pseudogley soils; influence of parent material age and land use. Geoderma 416 (5), 115801.

Thomen, A., Najafinobar, N., Penen, F., Kay, E., Upadhyay, P.P., Li, X., Phan, N.T.N., Malmberg, P., Klarqvist, M., Andersson, S., Kurczy, M.E., Ewing, A.G., 2020. Subcellular Mass Spectrometry Imaging and Absolute Quantitative Analysis across Organelles. ACS Nano 14 (4), 4316–4325.

Thompson, A., Chadwick, O.A., Rancourt, D.G., Chorover, J., 2006. Iron-oxide crystallinity increases during soil redox oscillations. Geochim. Cosmochim. Acta 70 (7), 1710–1727.

Thompson, A., Rancourt, D.G., Chadwick, O.A., Chorover, J., 2011. Iron solid-phase differentiation along a redox gradient in basaltic soils. Geochim. Cosmochim. Acta 75 (1), 119–133.

Trolard, F., Bourrie, G., Jeanroy, E., Herbillon, A.J., Martin, H., 1995. Trace metals in natural iron oxides from laterites: A study using selective kinetic extraction. Geochim. Cosmochim. Acta 59 (7), 1285–1297.

Vepraskas, M.J., 2001. Morphological Features of Seasonally Reduced Soils: Chapter 7, in: Richardson, J.L., Vepraskas, M.J. (Eds.), Wetland Soils. Genesis, Hydrology, Landscapes, and Classification. CRC Press, Boca Raton.

Vepraskas, M.J., Lindbo, D.L., 2012. Redoximorphic Features as Related to Soil Hydrology and Hydric Soils, in: Lin, H. (Ed.), Hydropedology. Synergistic Integration of Soil Science and Hydrology, vol. 7, 1st ed. Elsevier, Boston, pp. 143–172.

Vogelsang, V., Fiedler, S., Jahn, R., Kaiser, K., 2016a. In-situ transformation of iron-bearing minerals in marshland-derived paddy subsoil. Eur. J. Soil Science 67 (5), 676–685.

Vogelsang, V., Kaiser, K., Wagner, F.E., Jahn, R., Fiedler, S., 2016b. Transformation of clay-sized minerals in soils exposed to prolonged regular alternation of redox conditions. Geoderma 278, 40–48.

Weber, K.A., Achenbach, L.A., Coates, J.D., 2006. Microorganisms pumping iron: anaerobic microbial iron oxidation and reduction. Nat. Rev. Microbiol. 4 (10), 752–764.

Werner, F., Mueller, C.W., Thieme, J., Gianoncelli, A., Rivard, C., Hoeschen, C., Prietzel, J., 2017. Micro-scale heterogeneity of soil phosphorus depends on soil substrate and depth. Sci. Rep. 7 (1), 3203.

Williams, A.G.B., Scherer, M.M., 2004. Spectroscopic evidence for Fe(II)-Fe(III) electron transfer at the iron oxide-water interface. Environ. Sci. Technol. 38 (18), 4782–4790.

Winkler, P., Kaiser, K., Thompson, A., Kalbitz, K., Fiedler, S., Jahn, R., 2018. Contrasting evolution of iron phase composition in soils exposed to redox fluctuations. Geochim. Cosmochim. Acta 235, 89–102.

Wong, V.N.L., McNaughton, C., Pearson, A., 2016. Changes in soil organic carbon fractions after remediation of a coastal floodplain soil. J. Environ. Manage. 168, 280–287.

Young, I.M., Crawford, J.W., Nunan, N., Otten, W., Spiers, A., 2008. Microbial Distribution in Soils: Physics and Scaling: Chapter 4. Adv. Agron. 100, 81–121.

Yu, X., Lu, S., 2016. Micrometer-scale internal structure and element distribution of Fe-Mn nodules in Quaternary red earth of Eastern China. J. Soils Sediments 16 (2), 621–633.

Zack, G.W., Rogers, W.E., Latt, S.A., 1977. Automatic measurement of sister chromatid exchange frequency. J. Histochem. Cytochem. 25 (7), 741–753.

Zhang, M., Karathanasis, A.D., 1997. Characterization of Iron-Manganese Concretions in Kentucky Alfisols with Perched Water Tables. Clays Clay Miner. 45 (3), 428–439.

Appendix